VLF/LF TE-MODE PROPAGATION UNDER DISTURBED IONOSPHERIC CONDITIONS

Edward C. Field, et al

Pacific Sierra Research Corporation

Prepared for:

Air Force Cambridge Research Laboratories

July 1975

AFCRL-TR-75-0362

VLF/LF TE-MODE PROPAGATION UNDER DISTURBED IONOSPHERIC CONDITIONS

Edward C. Field and Michael A. Dore
Pacific-Sierra Research Corporation
1456 Cloverfield Boulevard
Santa Monica, California 90404

July 1975

Final Report for Period 1 May through 30 June 1975

AIR FORCE CAMBRIDGE RESEARCH LABORATORIES
AIR FORCE SYSTEMS COMMAND
UNITED STATES AIR FORCE
HANSCOM AFB, MASSACHUSETTS 01731

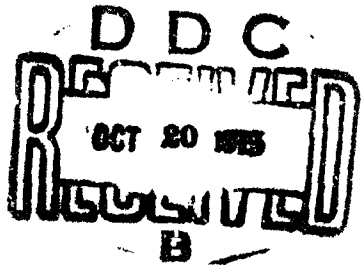

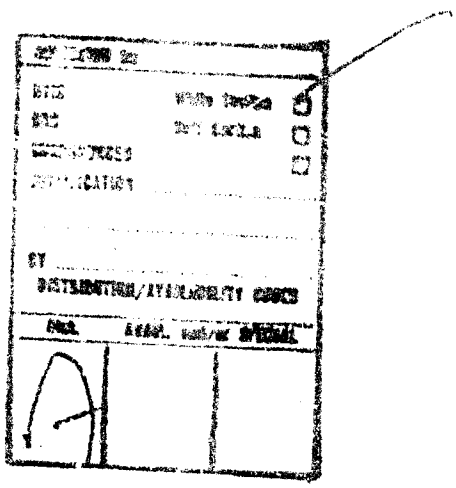

Qualified requestors may obtain additional copies from the Defense Documentation Center. All others should apply to the National Technical Information Service.

UNCLASSIFIED

SECURITY CLASSIFICATION OF THIS PAGE (When Data Entered)

REPORT DOCUMENTATION PAGE		READ INSTRUCTIONS BEFORE COMPLETING FORM
1 REPORT NUMBER AFCRL-TR-75-0382	2 GOVT ACCESSION NO	3 RECIPIENT'S CATALOG NUMBER
4 TITLE (and Subtitle) VLF/LF TE-MODE PROPAGATION UNDER DISTURBED IONOSPHERIC CONDITIONS		5 TYPE OF REPORT & PERIOD COVERED Final Report for period 1 May - 30 June 1975 6 PERFORMING ORG. REPORT NUMBER PSR-504
7 AUTHOR(s) Edward C. Field and Michael A. Dore		8 CONTRACT OR GRANT NUMBER(s) F19628-75-C-0181
9 PERFORMING ORGANIZATION NAME AND ADDRESS Pacific-Sierra Research Corporation 1456 Cloverfield Boulevard Santa Monica, California 90404		10 PROGRAM ELEMENT, PROJECT, TASK AREA & WORK UNIT NUMBERS 616A-00-99; 33131F; 678100
11 CONTROLLING OFFICE NAME AND ADDRESS Air Force Cambridge Research Laboratories Hanscom AFB, Massachusetts 01731 Monitor: Paul A. Kossey/LIE		12 REPORT DATE July 1975 13 NUMBER OF PAGES ~~56~~ 52
14 MONITORING AGENCY NAME & ADDRESS(if different from Controlling Office)		15 SECURITY CLASS (of this report) UNCLASSIFIED 15a DECLASSIFICATION/DOWNGRADING SCHEDULE --

16 DISTRIBUTION STATEMENT (of this Report)

Approved for public release; distribution unlimited.

17 DISTRIBUTION STATEMENT (of the abstract entered in Block 20, if different from Report)

18 SUPPLEMENTARY NOTES

19 KEY WORDS (Continue on reverse side if necessary and identify by block number)

VLF Propagation
Strategic Communications
Nuclear Effects

20 ABSTRACT (Continue on reverse side if necessary and identify by block number)

This report compares calculated attenuation rates for transverse magnetic (TM) and transverse electric (TE) modes propagating in the earth-ionosphere waveguide. Frequencies from 10 to 50 kHz are considered, and attention is restricted to situations where the fields can be represented in terms of the least-attenuated TM or TE mode. Nine model ionospheres corresponding to conditions caused by widespread high-altitude fission debris are used as inputs to the calculations. Certain of these models are also representative of polar-cap-absorption (PCA)

DD FORM 1 JAN 73 1473 EDITION OF 1 NOV 65 IS OBSOLETE

UNCLASSIFIED

SECURITY CLASSIFICATION OF THIS PAGE (When Data Entered)

20. ABSTRACT (cont'd)

events. The calculations utilize full-wave methods, and account for the vertical inhomogeneity of the ionosphere, the effects of heavy ions, and the curvature of the earth. In addition to the modal attenuation rates, results are given for field-strength height-profiles, plane-wave ionospheric reflection coefficients, and the relative importance of heavy ions *vis-à-vis* electrons.

SUMMARY

This report compares calculated attenuation rates for transverse magnetic (TM) and transverse electric (TE) modes propagating in the earth-ionosphere waveguide. Frequencies from 10 to 50 kHz are considered, and attention is restricted to situations where the fields can be represented in terms of the least-attenuated TM or TE mode. Nine model ionospheres corresponding to conditions caused by widespread high-altitude fission debris are used as inputs to the calculations. Certain of these models are also representative of polar-cap-absorption (PCA) events. The calculations utilize full-wave methods, and account for the vertical inhomogeneity of the ionosphere, the effects of heavy ions, and the curvature of the earth. In addition to the modal attenuation rates, results are given for field-strength height-profiles, plane-wave ionospheric reflection coefficients, and the relative importance of heavy ions *vis-à-vis* electrons.

PREFACE

This report compares transverse electric (TE) and transverse magnetic (TM) mode attenuation in the earth-ionosphere waveguide for frequencies between 10 and 50 kHz. A wide variety of disturbed ionospheres characteristic of nuclear environments and polar-cap-absorption (PCA) events are considered. The results are of interest in the context of elevated antennas having a significant horizontally oriented component.

CONTENTS

FIGURES

FIGURES

I. INTRODUCTION

Under most conditions, only transverse magnetic (TM) modes are of practical interest for the propagation of VLF/LF waves in the earth-ionosphere waveguide. The transverse electric (TE) modes are typically more highly attenuated and more difficult to generate from ground-based transmitting antennas. Thus, TM-mode attenuation in ambient and disturbed environments has been thoroughly studied and documented (e.g., Field, 1965; Knapp and Swanberg, 1973). For elevated, horizontally oriented transmitting antennas, however, the TE mode could be preferable to the TM mode under certain conditions. Accordingly, this report presents comparisons between TE- and TM-mode attenuation rates for frequencies between 10 and 50 kHz. We consider a wide variety of disturbed ionospheres characteristic of nuclear environments and polar-cap-absorption (PCA) events. In addition to the calculated attenuation rates, results are given for field-strength height-profiles, plane-wave reflection coefficients, and the relative importance of heavy ions vis-à-vis electrons.

Section II presents and discusses the ionospheric models used; Sec. III, calculated TE- and TM-mode attenuation rates for ambient and disturbed conditions as well as field-strength height-profiles for the two types of modes; Sec. IV, TE and TM plane-wave reflection coefficients for ambient and disturbed conditions; and Sec. V, results illustrating the sensitivity of the propagation to ion mass, collision frequency, and number density. The equations and computer codes used are summarized in the appendix.

II. AMBIENT AND DISTURBED IONOSPHERIC MODELS

The ambient daytime electron and ion density-profiles used (see Fig. 1) in the calculations are taken from Knapp and Schwartz (1975). The electron-neutral collision-frequency profile (Fig. 2) comes from the same reference. The ion-neutral collision frequency, ν_i, is uncertain, and is believed to lie between 1/10 and 1/40 of the electron-neutral collision frequency, ν_e. Except where otherwise stated, the calculations assume singly ionized ions having an atomic mass number of 29 and an ion-to-electron collision frequency ratio of 1/40.

The assumed nuclear environments correspond to fission debris uniformly spread over a wide area at altitudes above, say, 150 km or so. The parameter, W, used to characterize the debris-ionizing intensity is given by

$$W = \frac{Y_F}{A(1+t)^{1.2}} \quad , \tag{1}$$

where

Y_F = total deposited fission yield in megatons,

A = area over which debris is uniformly spread in $(\text{kilometers})^2$,

t = time after burst in seconds.

Strictly speaking, Eq. (1) applies only to situations in which all bursts occur at t = 0. For a large number of bursts at different times, one can express W as a sum of $Y_F/(1+t)^{1.2}$ terms and determine an equivalent value for any time. However, the purpose of this report is to compare TE- and TM-mode propagation over a wide range of environments,

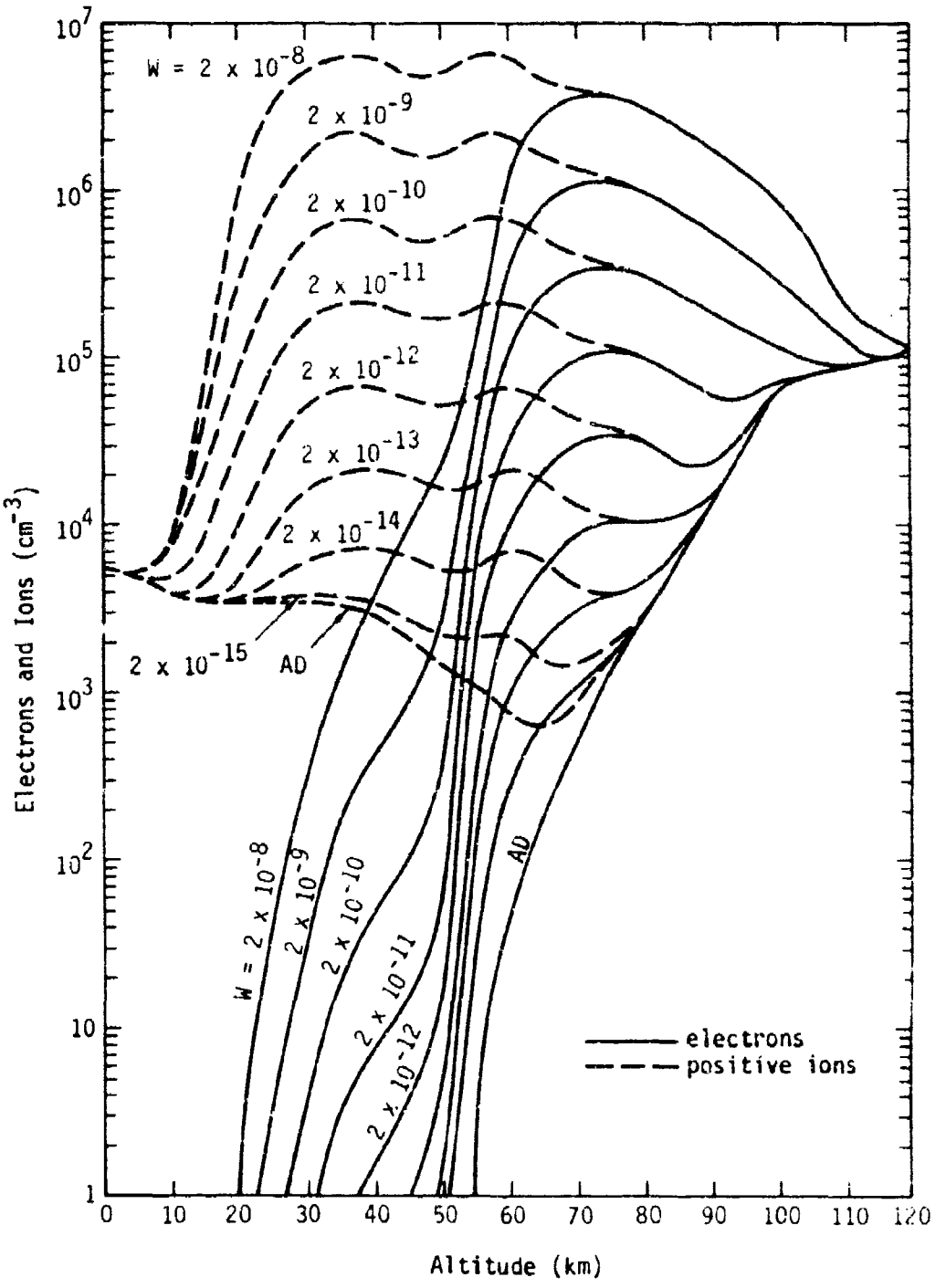

Fig. 1--Electron- and ion-density profiles for daytime ambient (AD) and disturbed environments.

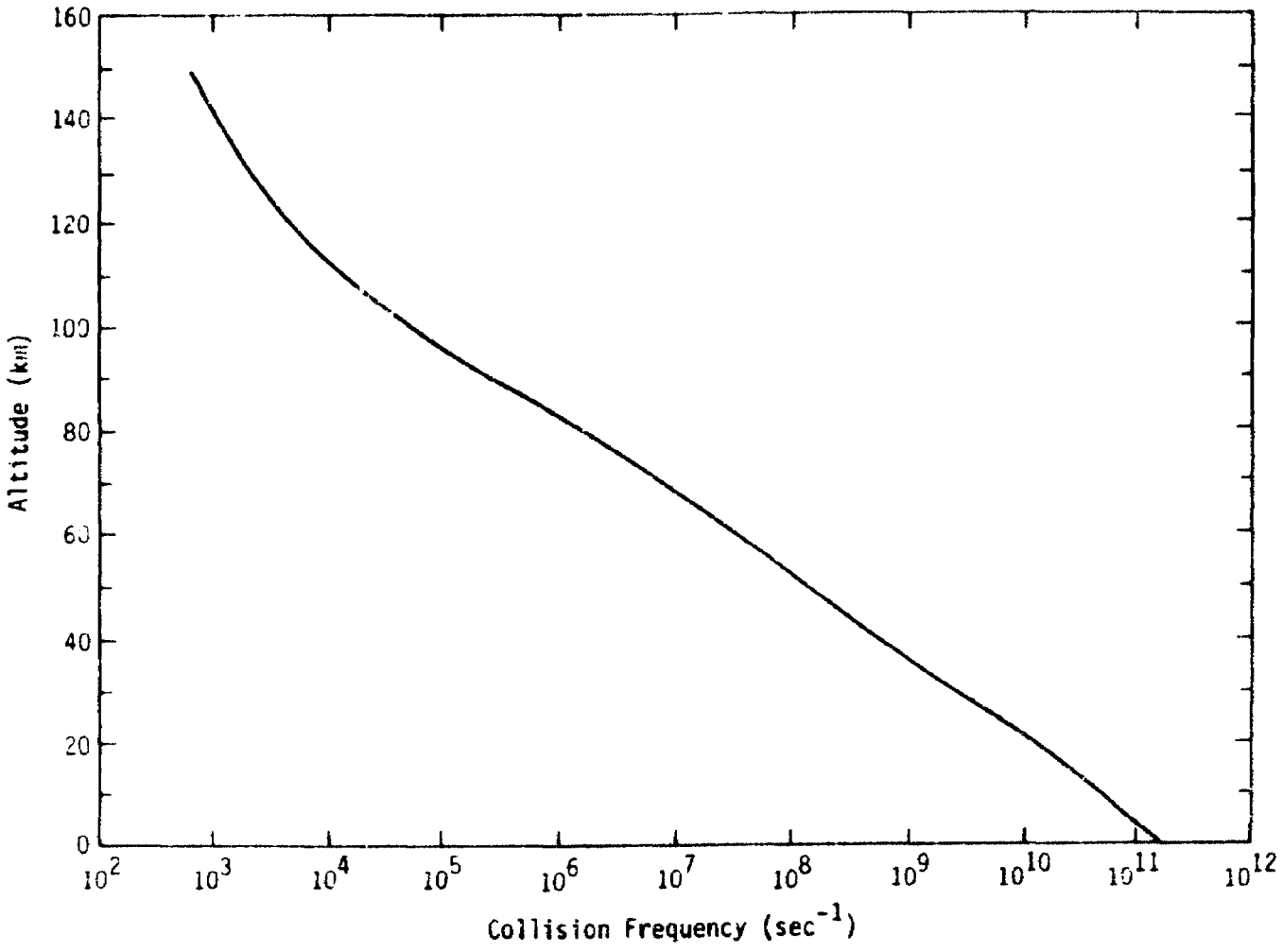

Fig. 2--Electron collision frequency.

rather than to draw detailed conclusions for specific scenarios. The parameter W is a simple yet realistic one with which to characterize such a range of environments. For example, a value for W of 10^{-8} represents a severe environment, values between 10^{-10} and 10^{-11} characterize moderate environments, and smaller values characterize weak environments.

Figure 3 illustrates the normalized, nominal ion-pair production-rate height-profile due to a uniform layer of high-altitude debris. The peaks at about 30 and 65 km are due to gamma and beta radiation, respectively. The actual production rate for a given environment can be obtained by multiplying the curve in Fig. 3 by $2.5 \times 10^{14} W$; i.e., the peak production is $2.5 \times 10^{14} W$ ion-pairs/cm^3-sec and occurs at 65 km.

Figure 1 shows daytime electron and ion density-profiles for values of W from 2×10^{-15} to 2×10^{-8}. These profiles were obtained by using the production rates, as determined above, as inputs to the quasi-equilibrium form of the ionization balance equations. A simple lumped-parameter model was used for the various reaction-rate coefficients.*

Although the profiles shown in Fig. 1 apply strictly to spread-debris environments, they cover a range of ionization levels reasonably representative of other types of nuclear and non-nuclear disturbances. For example, the $W = 2 \times 10^{-12}$ profile is somewhat similar to that caused by a strong PCA event (e.g., *Field, 1970*).

---

*Specifically, Eqs. (22-25) to (22-27) and Table 22-5 as given in Ali, Knapp, and Niles (*1975*) are used in the calculation of the profiles shown in Fig. 1.

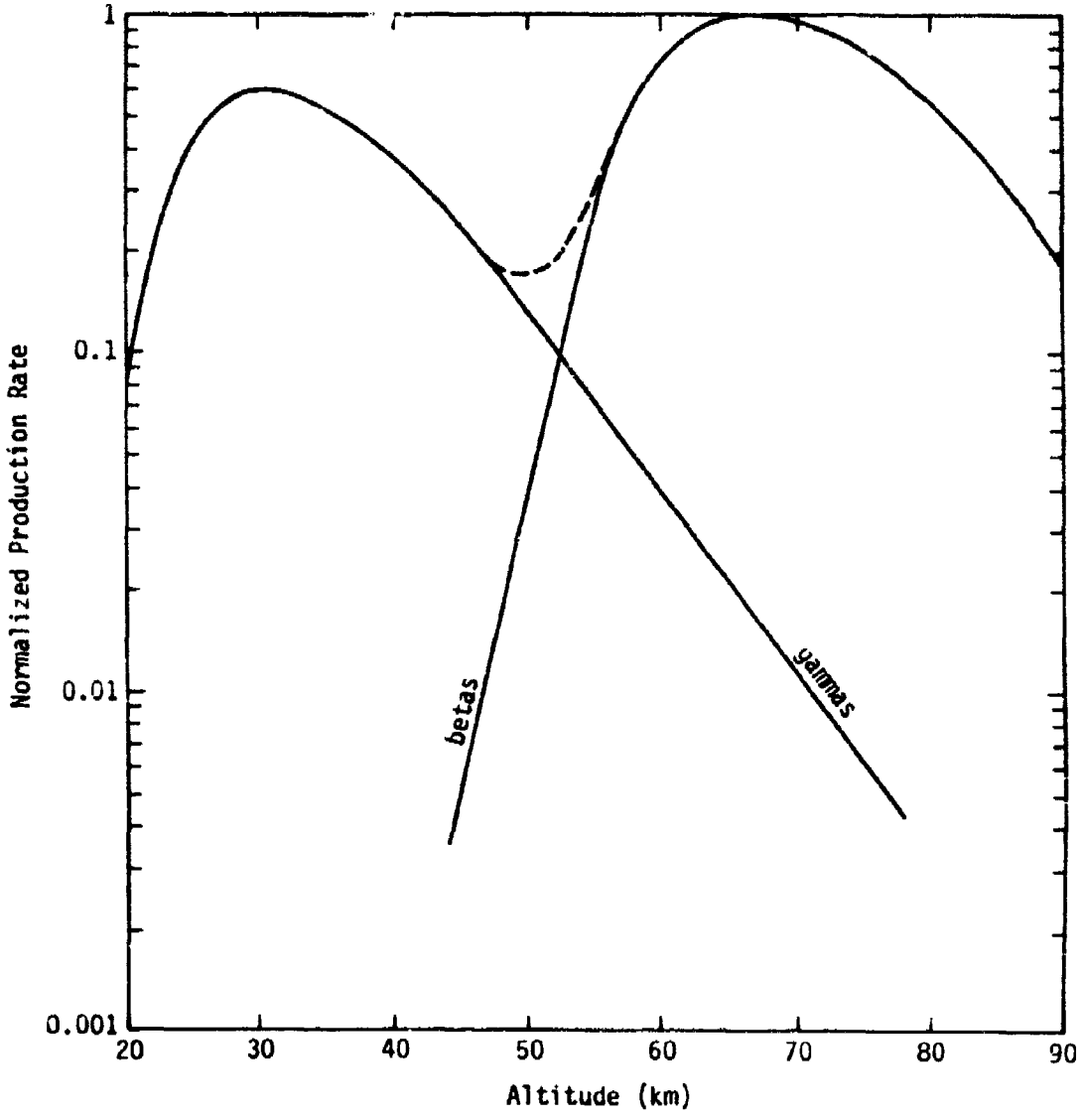

Fig. 3--Ion-pair production rate for high-altitude fission debris.

III. TE AND TM MODES

ATTENUATION RATES

The attenuation rates of the dominant TE and TM modes have been calculated for each of the model density-profiles shown in Fig. 1. For the more highly disturbed cases, calculations are made for frequencies between 10 to 50 kHz. For the roughly 2000- to 10,000-km path lengths of interest here, the representation of the field in terms of only the least-attenuated mode becomes invalid for frequencies above 30 kHz and mildly disturbed or ambient conditions. This lack of validity occurs because--unlike for moderate or severe environments--in the LF and upper VLF bands, the attenuation rates of higher-order modes are comparable with that of the lowest mode. Thus, for $W \leq 2 \times 10^{-14}$, 30 kHz is the highest frequency for which calculations are performed.

Figure 4 shows the attenuation rate of the least-attenuated TM mode as a function of W for several VLF and LF frequencies. These results correspond very closely to calculated TM-mode attenuation rates reported by GE TEMPO in *Aids for the Study of Electromagnetic Blackout (1975)*. Figure 5 shows analogous results for the least-attenuated TE mode. Comparing Figs. 4 and 5 reveals that, for all cases shown, the TE mode is more heavily attenuated than the TM mode. In the VLF band ($\leq$30 kHz), the TE-mode attenuation becomes prohibitive for environments characterized by an ionizing-intensity parameter, W, greater than about 2×10^{-11}.

A more detailed comparison between TM- and TE-mode attenuation can be made from Figs. 6 through 14, which show the attenuation rates of the lowest-order TE and TM modes versus frequency for each of the model

profiles of Fig. 1. For mildly disturbed or undisturbed conditions (Figs. 6 through 10), the TE-mode attenuation rate exceeds that of the TM mode by no more than a few dB/Mm. Moreover, in the LF band (frequency ≥30 kHz), the difference between TE- and TM-mode attenuation rates is only 1 or 2 dB/Mm. In these cases, the TE mode could be preferred for an elevated transmitting antenna having a mainly horizontal orientation. For moderately and severely disturbed environments (Figs. 11 through 14), the TE mode is much more heavily attenuated than the TM mode for the frequencies considered. In these cases, the TM mode appears dominant except for almost perfectly horizontal (electric dipole) transmitting antennas.

FIELD-STRENGTH PROFILES

To assess the performance of elevated receivers, it is useful to examine the height-profiles of the electric and magnetic field strengths. Accordingly, these profiles are calculated for the least-attenuated TM and TE modes for all model ionospheres and wave frequencies for which attenuation rates are shown above. In the interest of brevity, only a few sample profiles will be shown here.

Figures 15 and 16 show the absolute values of the calculated field-strength profiles for the TM and TE modes, respectively. $W = 2\times10^{-12}$ and $f = 35$ kHz were chosen because, for these parameters, the TE-mode attenuation is only about 2.5 dB/Mm larger than the TM-mode attenuation (Fig. 10). The r- and ϕ-components of the fields exhibit the classic TM- and TE-mode structure, whereas the θ-component exhibits a minimum at an intermediate altitude. Had the real part of the calculated fields, rather than the absolute values, been plotted, the

θ-component height-profile would exhibit a more conventional structure. The absolute value gives the maximum field strength that could occur at each height. This maximum, of course, depends on the phase of the signal and will occur at different phases for different heights.

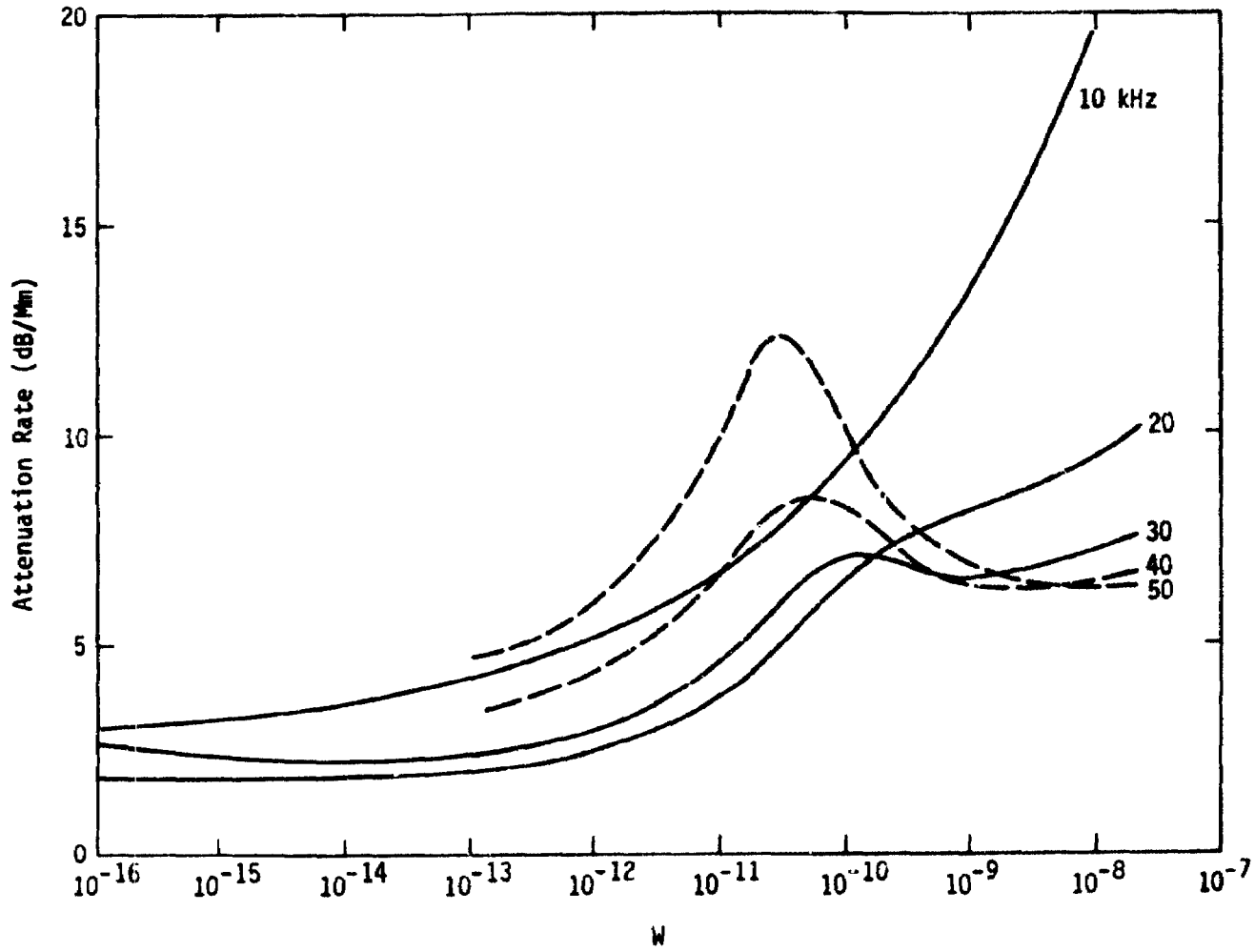

Fig. 4--Daytime attenuation rates for the lowest-order TM mode.

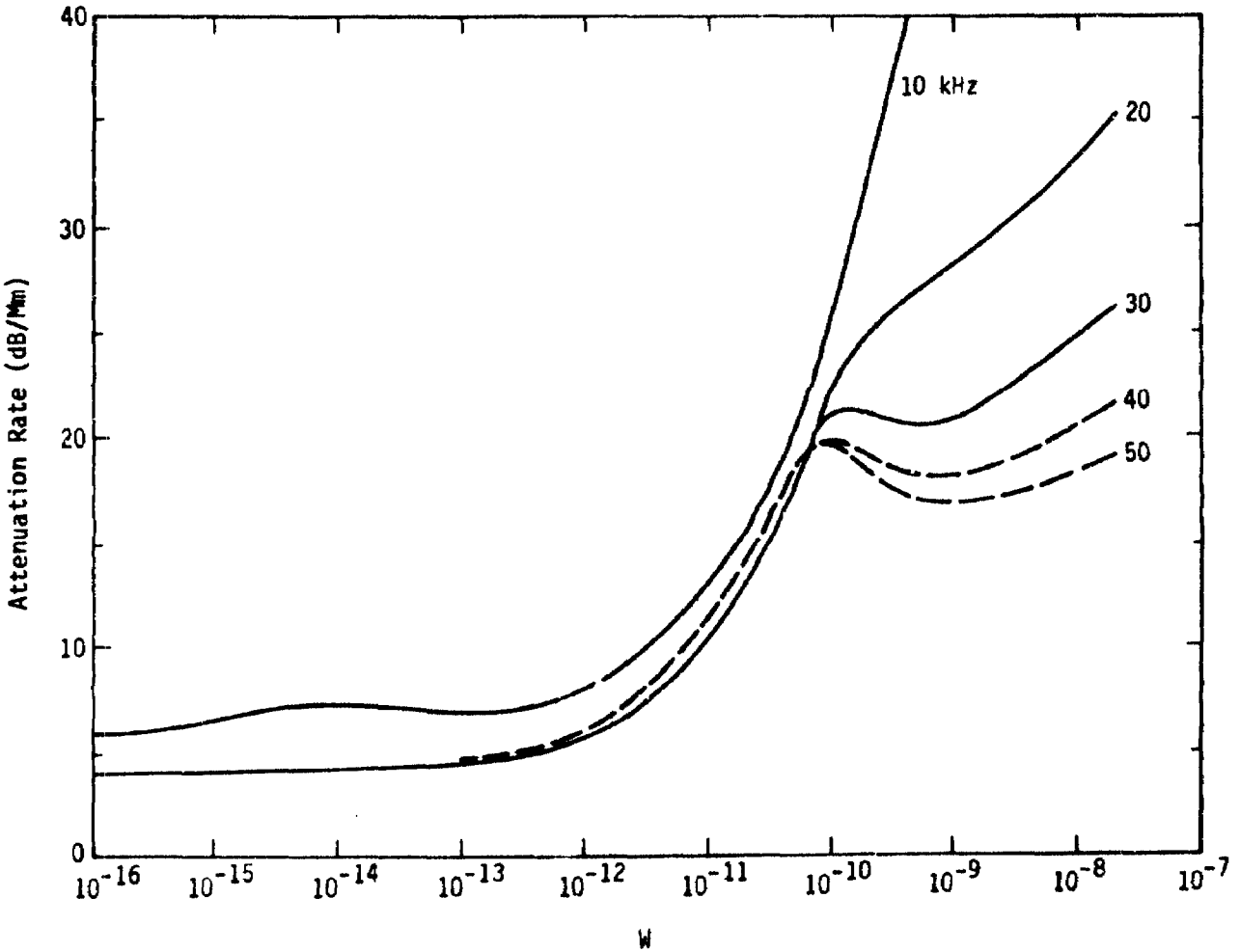

Fig. 5--Daytime attenuation rates for the lowest-order TE mode.

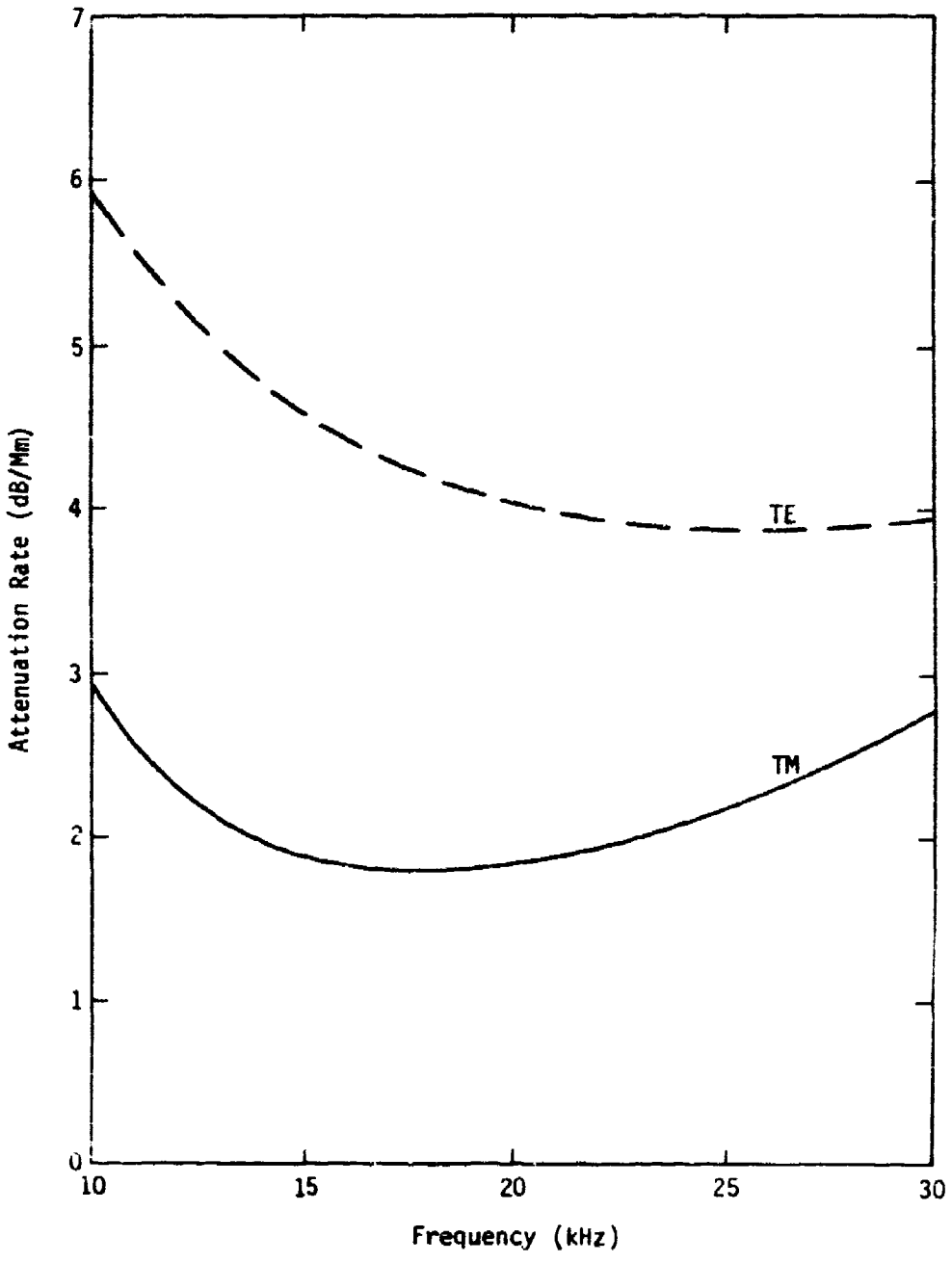

Fig. 6--Attenuation rate versus frequency for ambient day.

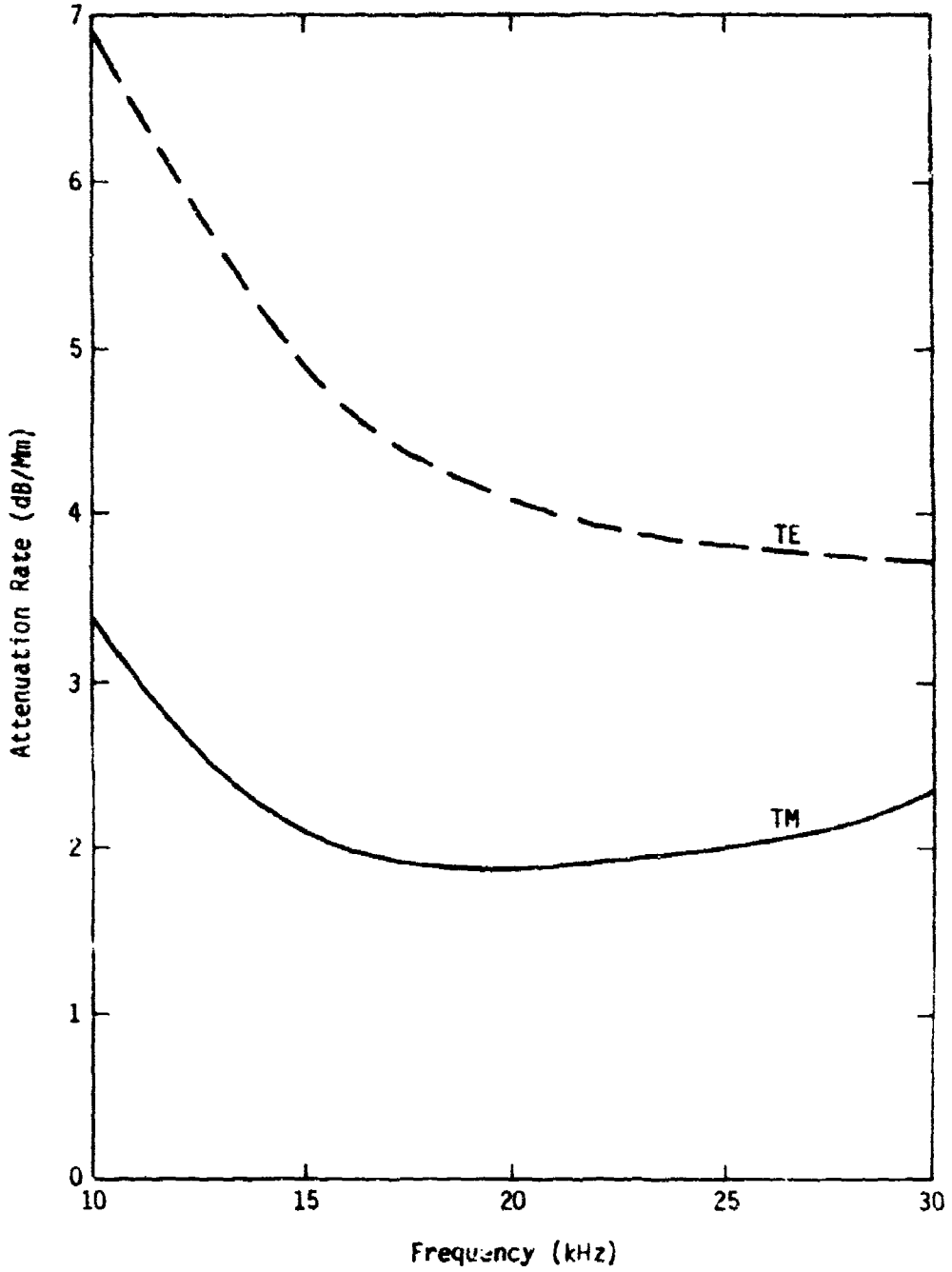

Fig. 7--Attenuation rate versus frequency for $\Sigma = 2\times10^{-15}$.

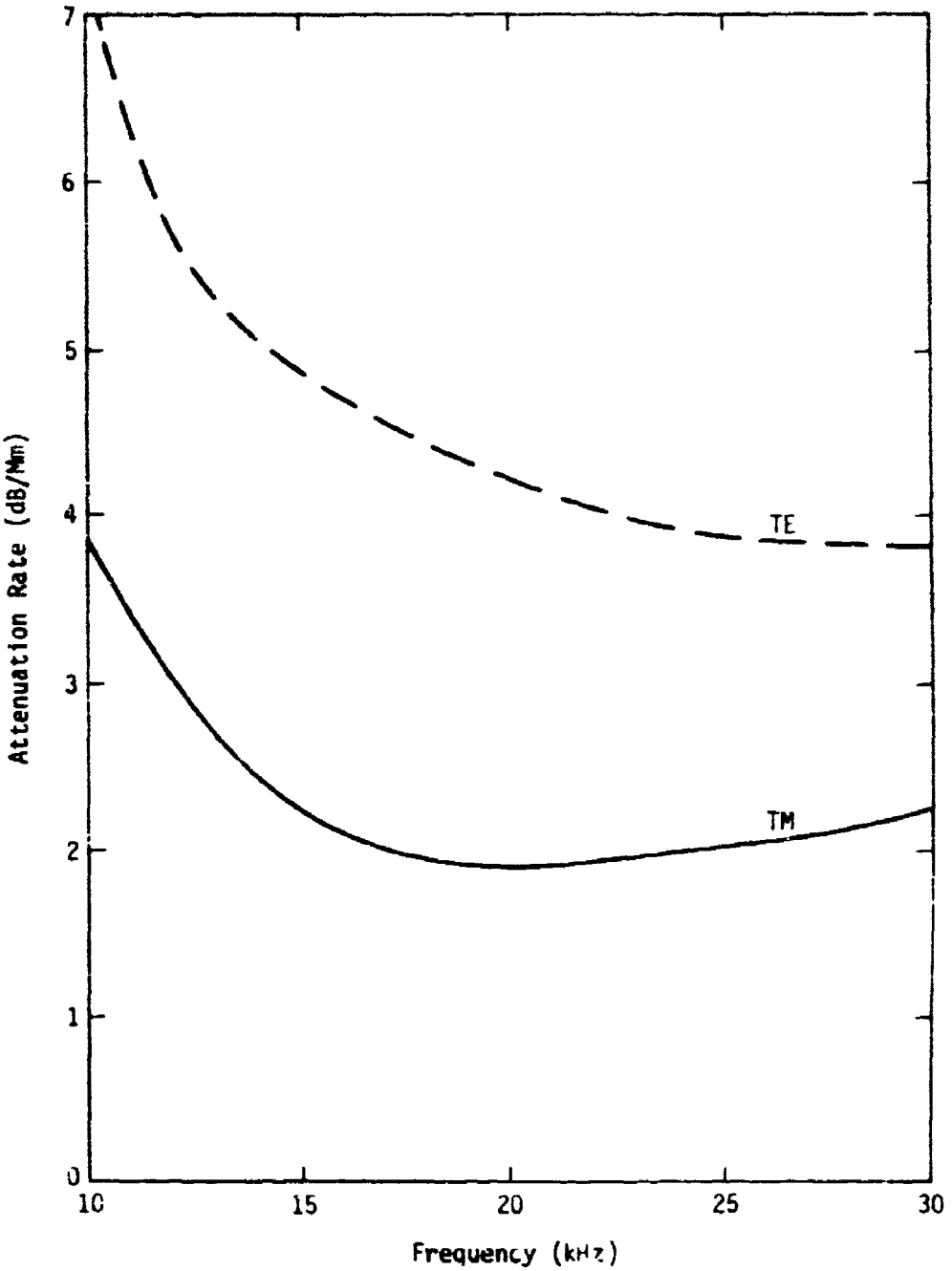

Fig. 8--Attenuation rate versus frequency for $W = 2 \times 10^{-14}$.

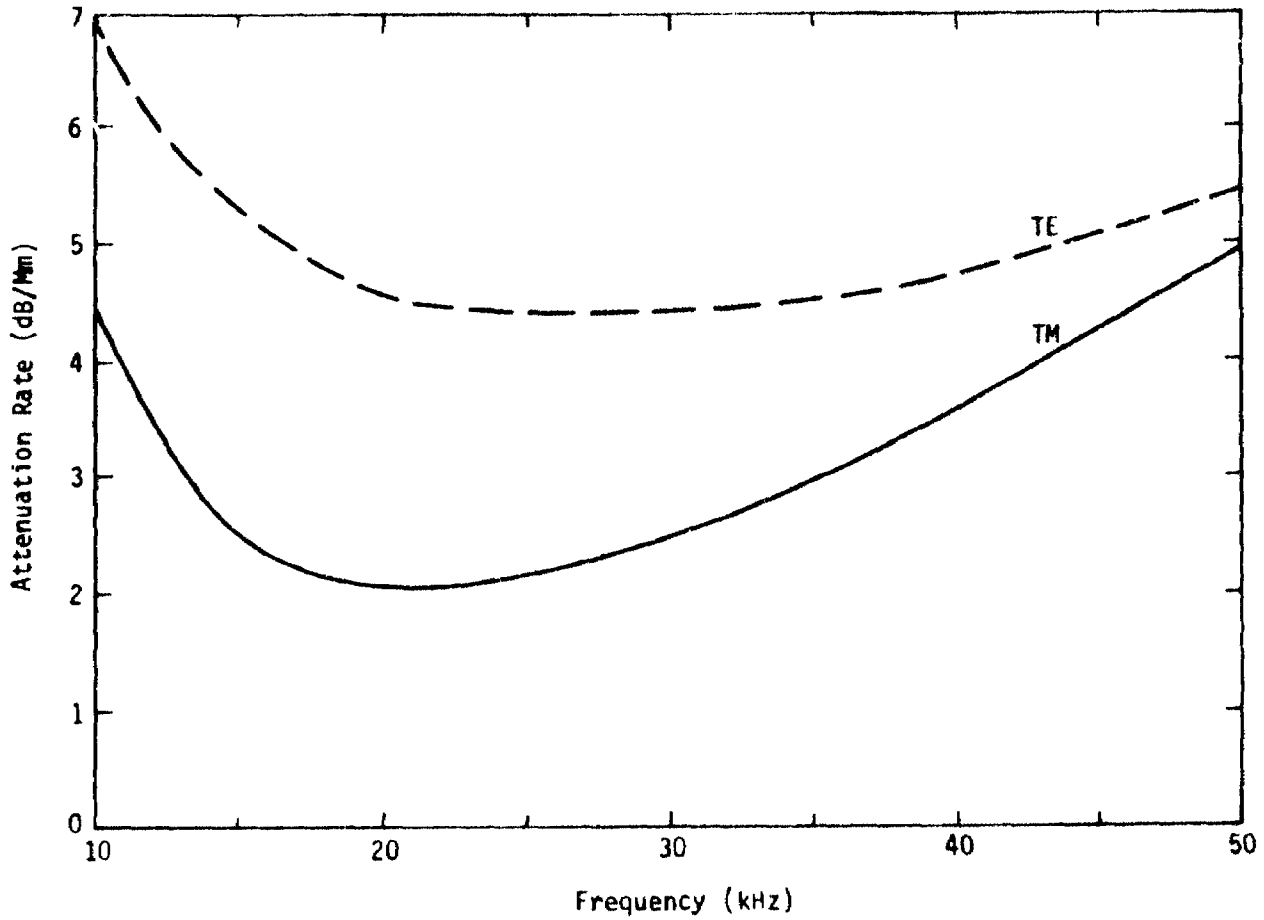

Fig. 9 -Attenuation rate versus frequency for $W = 2 \times 10^{-13}$.

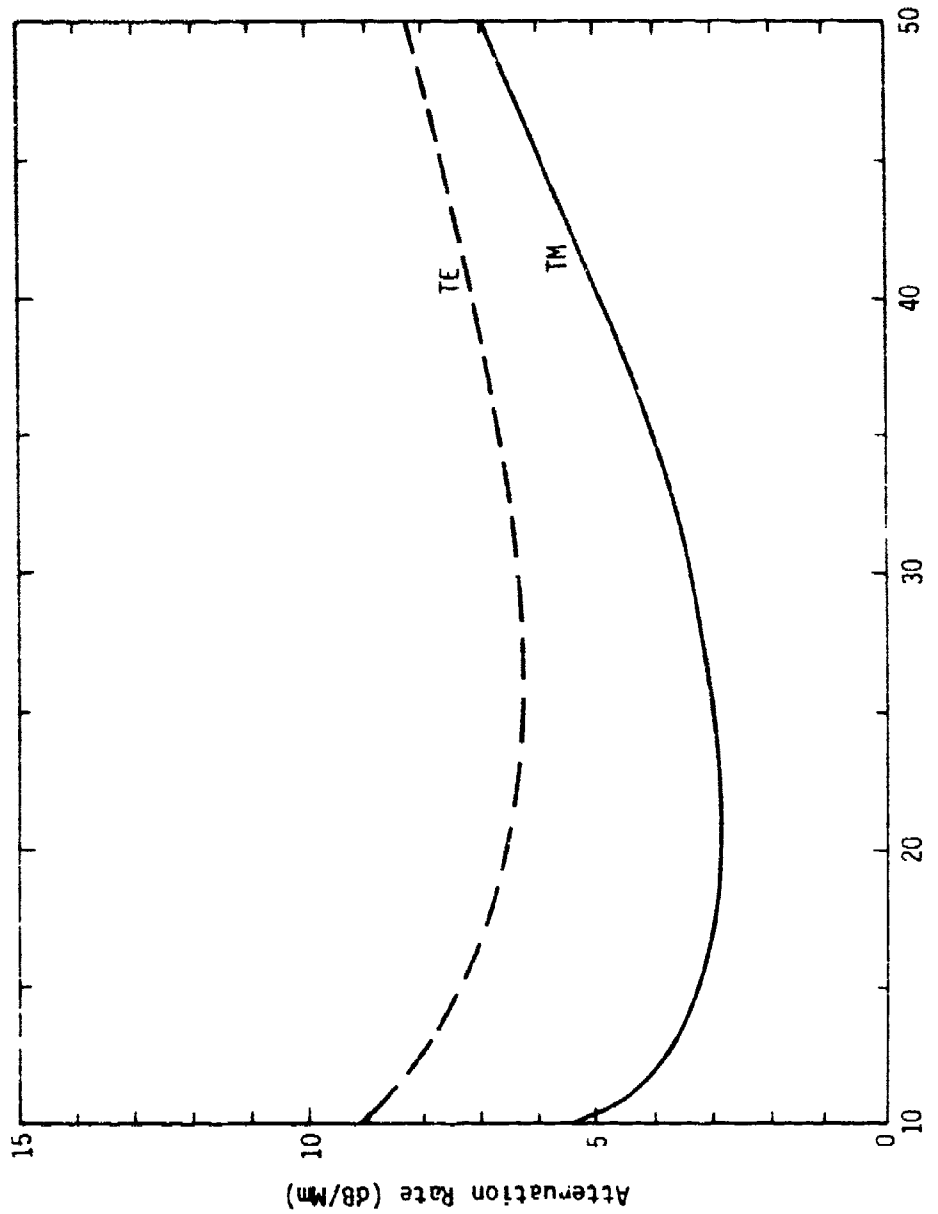

Fig. 10--Attenuation rate versus frequency for $N = 2 \times 10^{-12}$.

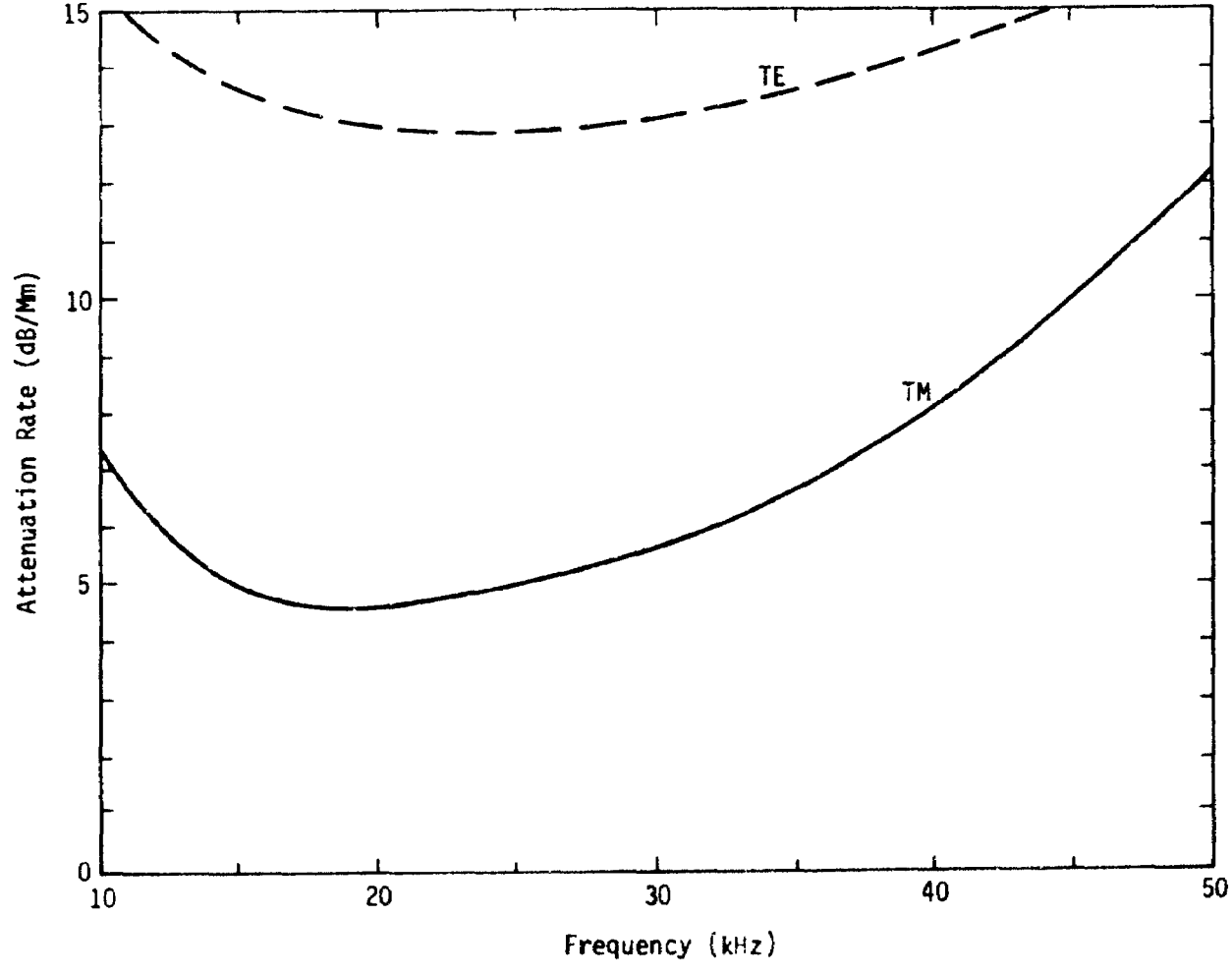

Fig. 11--Attenuation rate versus frequency for $W = 2 \times 10^{-11}$.

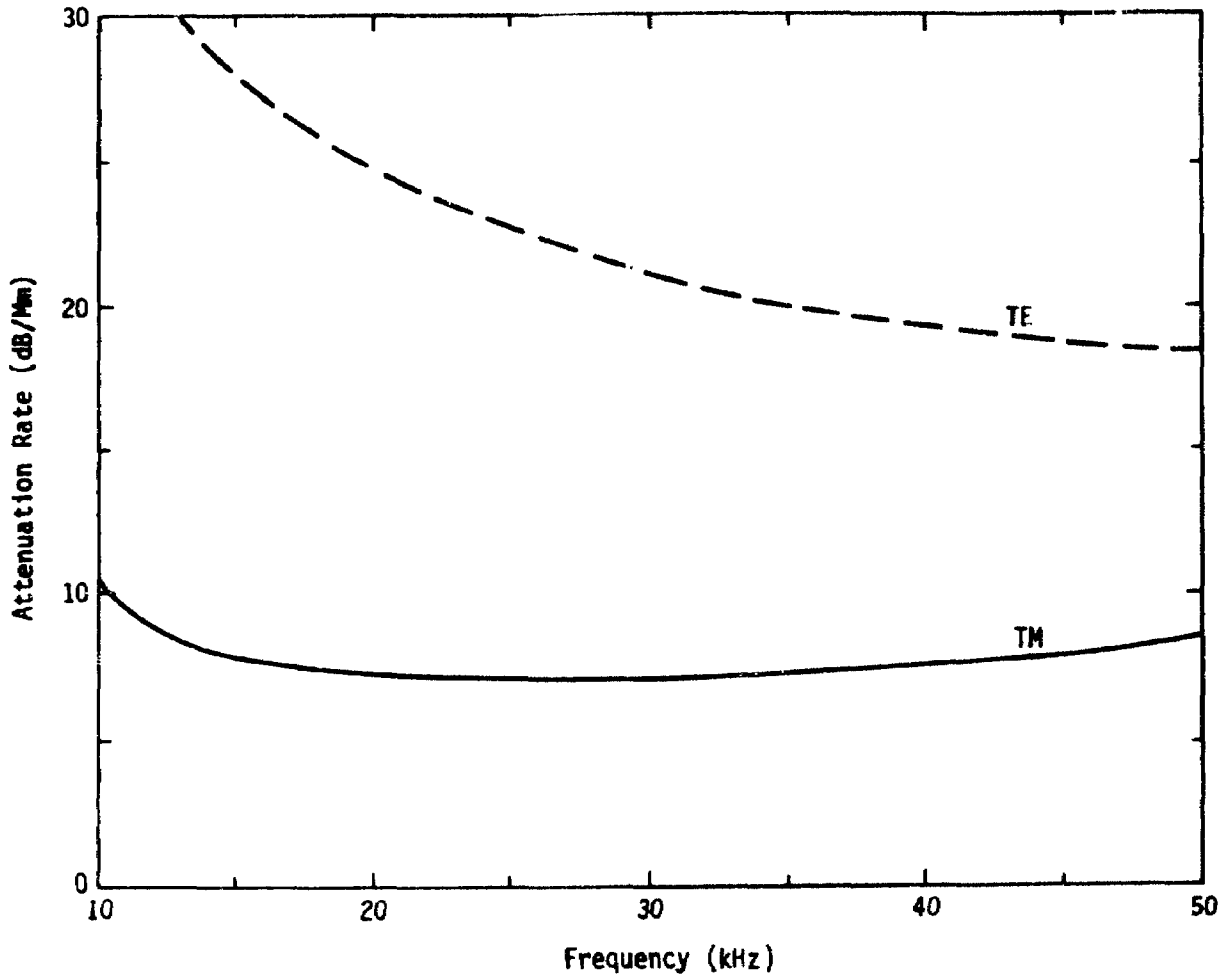

Fig. 12--Attenuation rate versus frequency for $W = 2 \times 10^{-10}$.

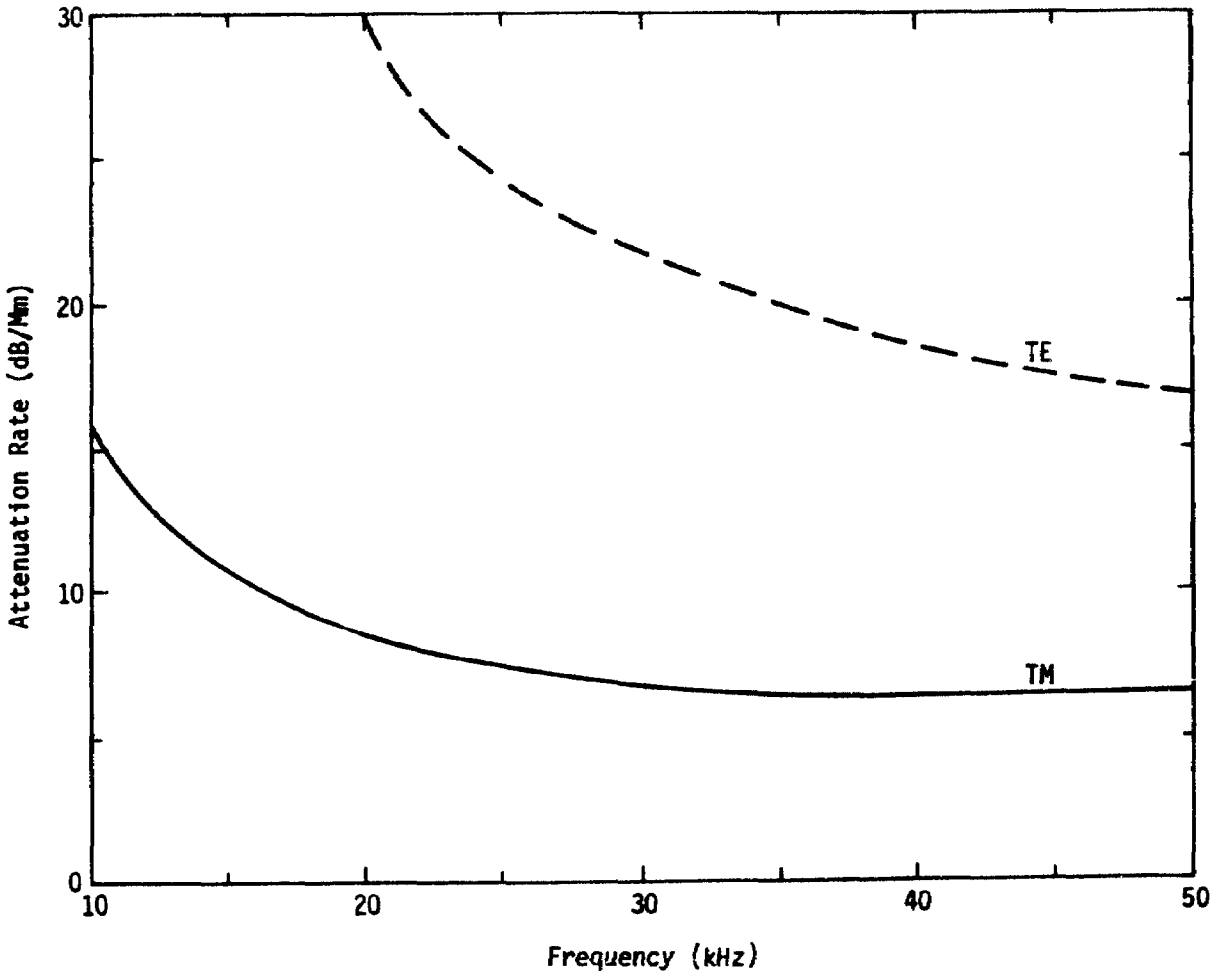

Fig. 13--Attenuation rate versus frequency for $W = 2 \times 10^{-9}$.

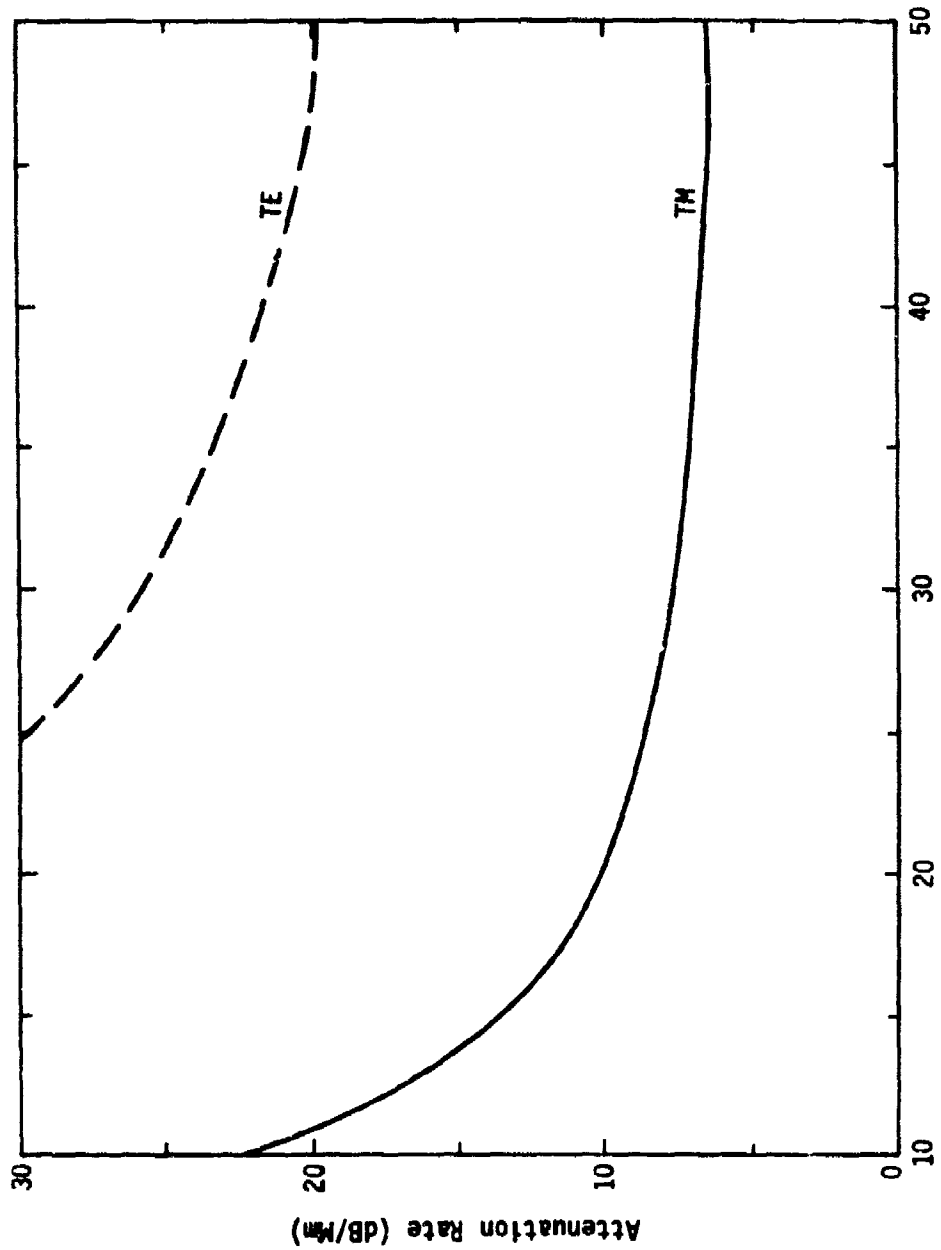

Fig. 14--Attenuation rate versus frequency for W = 2×10^{-8}.

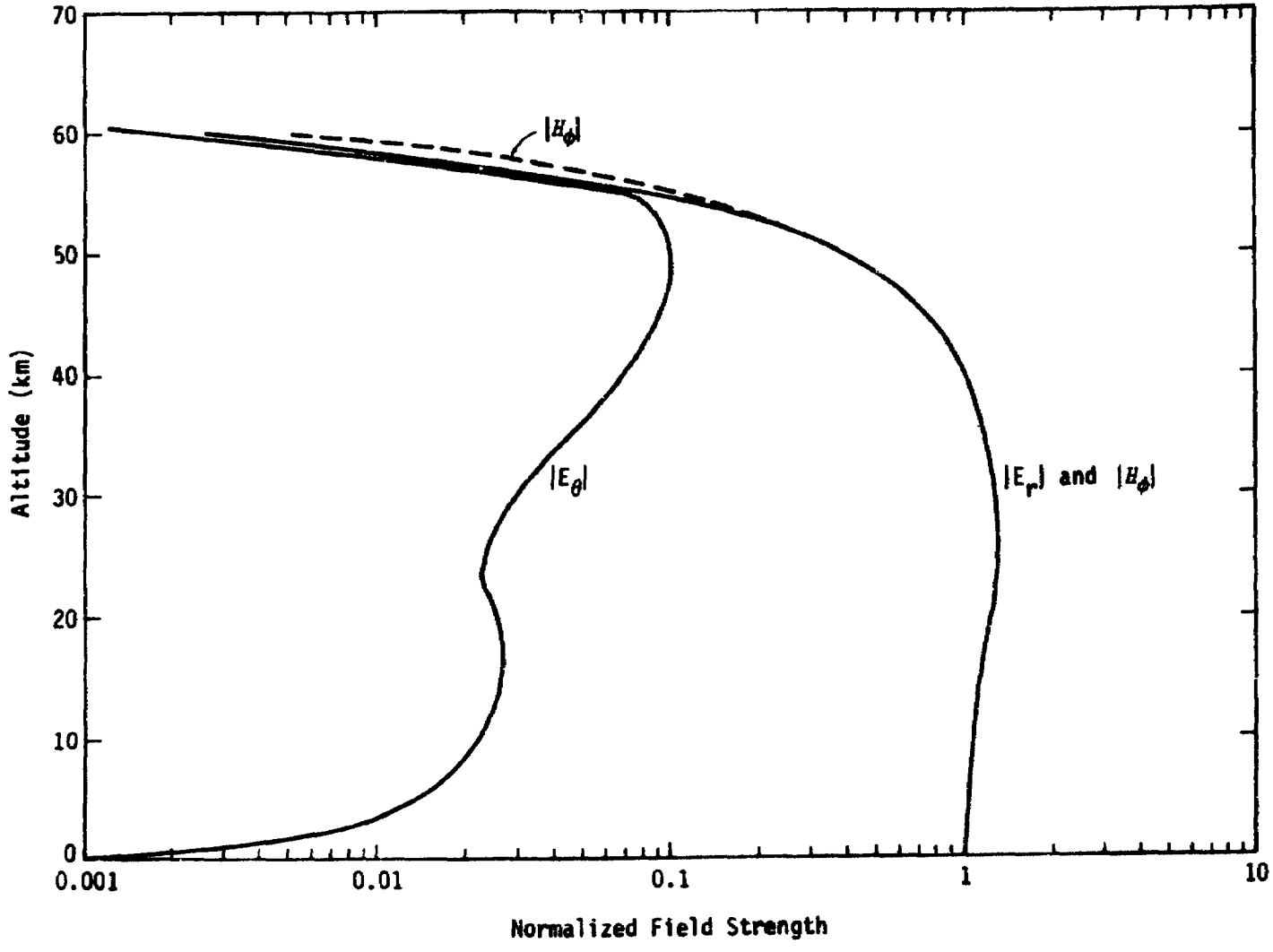

Fig. 15--TM-mode field-strength profiles for 35 kHz and W = 2×10^{-12}.

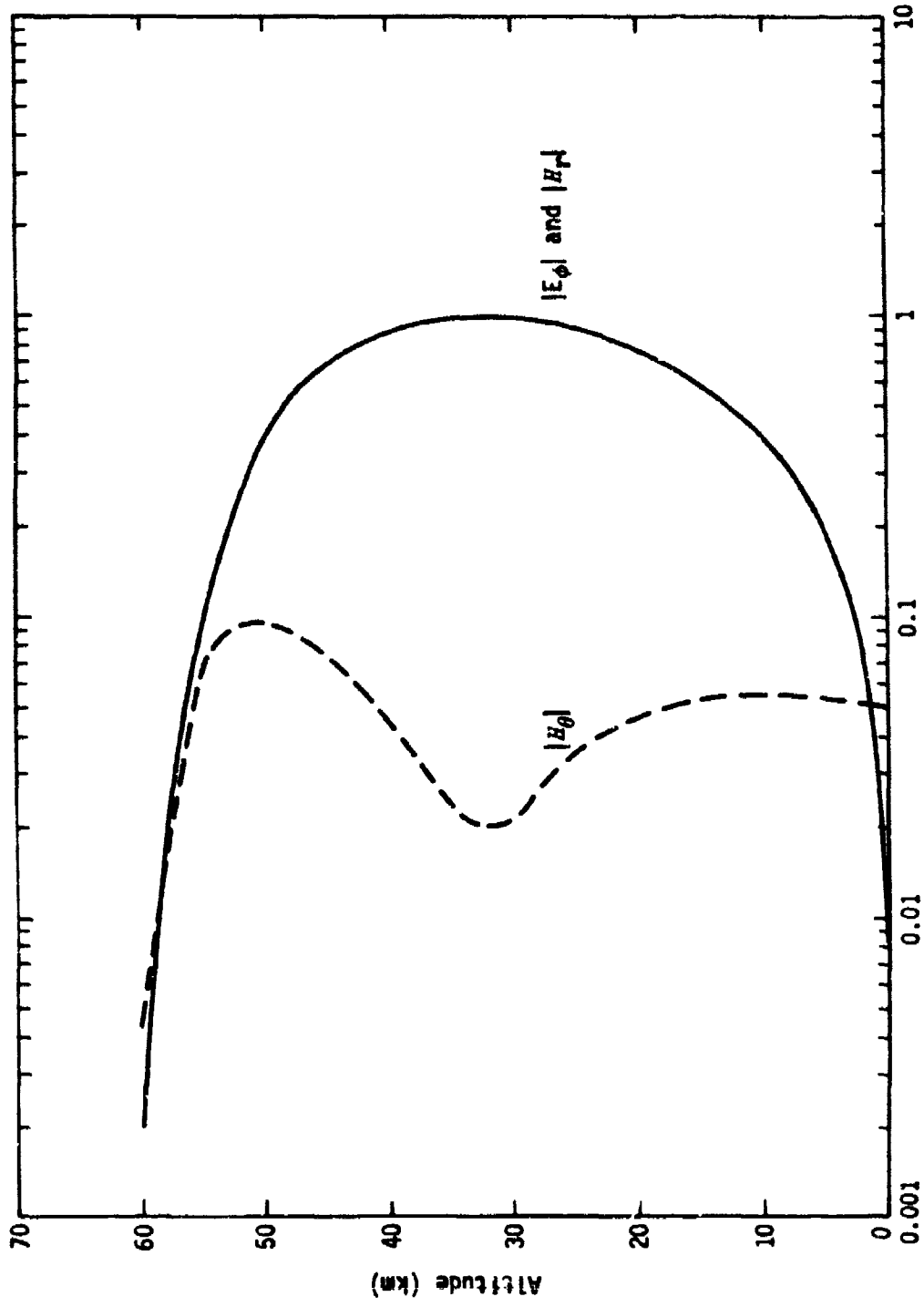

Fig. 16--TE-mode field-strength profiles for 35 kHz and $W = 2 \times 10^{-12}$.

IV. REFLECTION COEFFICIENTS

Figures 17 through 20 show the TM (E-vector in plane of incidence) and TE (E-vector perpendicular to plane of incidence) reflection coefficients at 20 kHz versus the cosine, C, of the incidence angle for ambient conditions and disturbed environments characterized by W = 2×10^{-13}, 2×10^{-11}, and 2×10^{-9}, respectively. For the ambient and mildly disturbed cases (Figs. 17 and 18), the reflection coefficients exhibit the classic behavior; *viz*, the TE coefficient decreases monotonically as C increases, whereas the TM coefficient exhibits a quasi-Brewster angle. However, each coefficient exhibits a minimum for the more strongly disturbed environments (Figs. 19 and 20). The reasons for this anomalous behavior are discussed below.

Figures 21 through 24, which correspond to Figs. 17 through 20, show the height dependence of the reflection coefficients for normal incidence (C = 1) and an oblique incidence angle of 78.46° (C = 0.2) representative of a waveguide mode eigenangle. As discussed in the appendix, $|R|$ is correctly interpreted as the ratio of downcoming to upgoing waves only below those altitudes at which reflections can occur; i.e., below the sensible ionosphere for the frequency and incidence angle in question. Stated differently, $|R|$ is a true reflection coefficient at altitudes where it has become independent of z. Thus, for ambient conditions (Fig. 21), significant reflections occur down to about 55 to 60 km, whereas for W = 2×10^{-9} (Fig. 24) they occur at altitudes as low as 25 to 30 km.

To understand the form of the reflection coefficients shown in Figs. 17 through 20, it is instructive to examine the height dependence

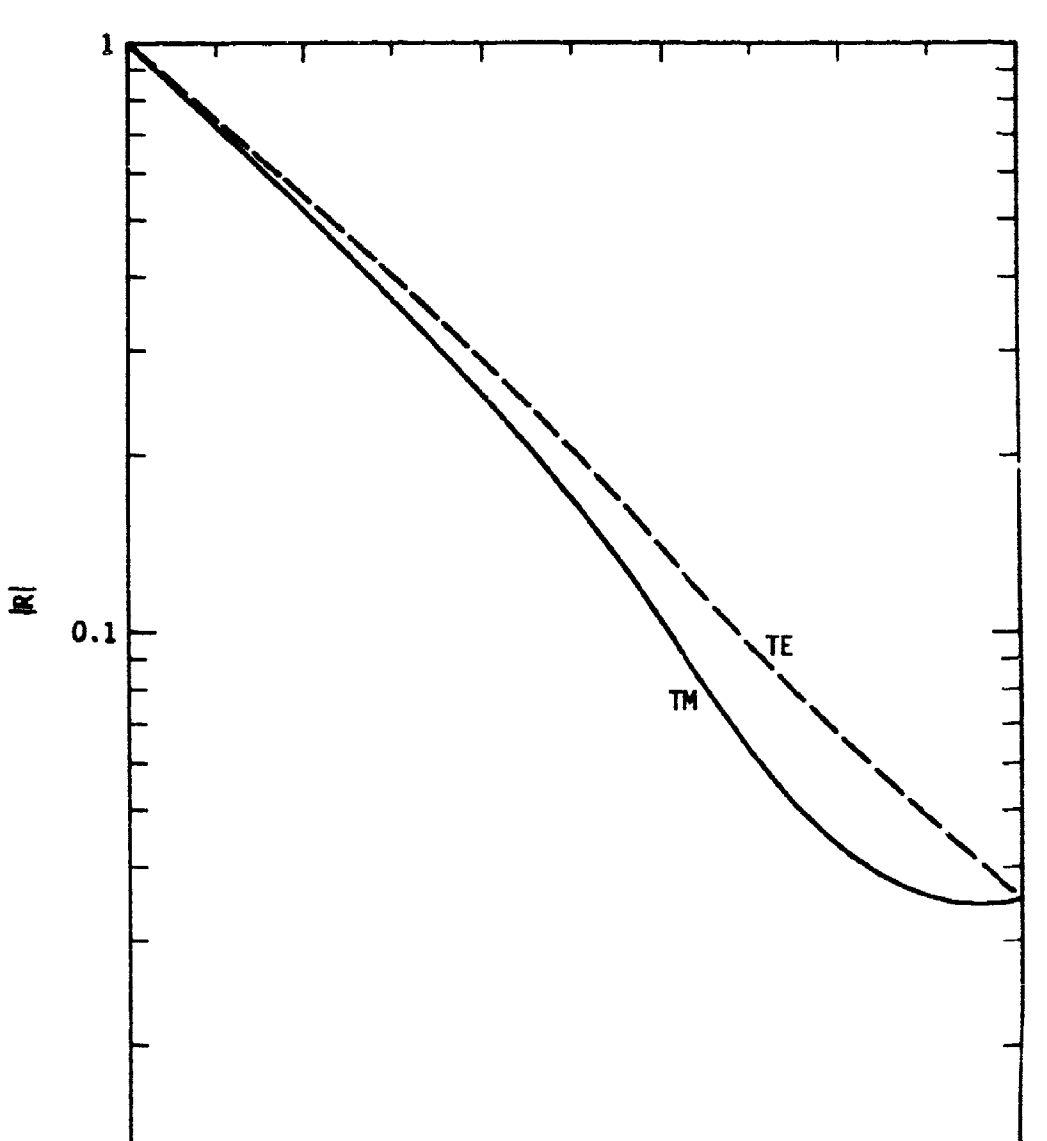

Fig. 17--Reflection coefficients versus incidence angle at 20 kHz, ambient day.

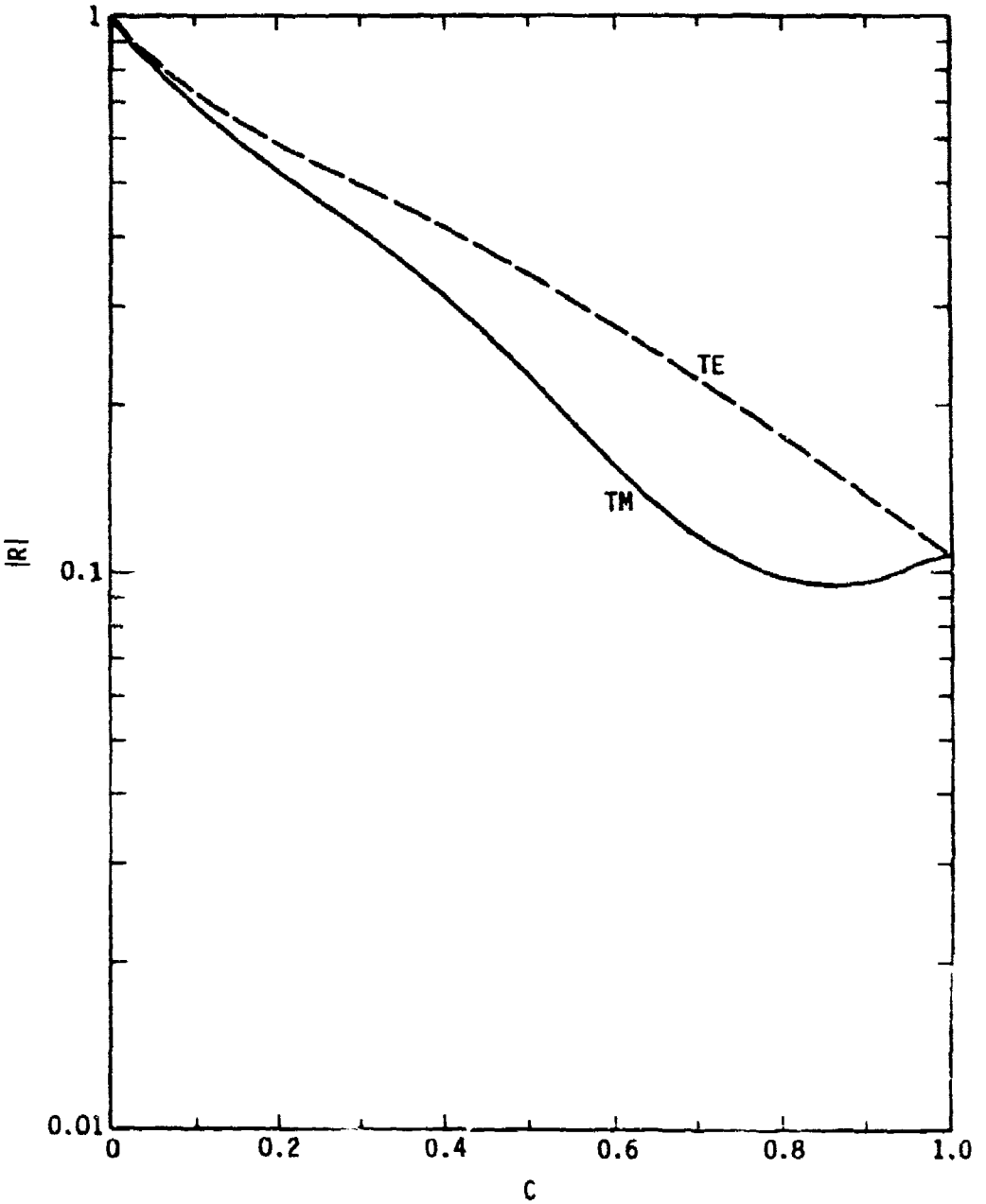

Fig. 18--Reflection coefficients versus incidence angle at 20 kHz, W = 2×10^{-13}.

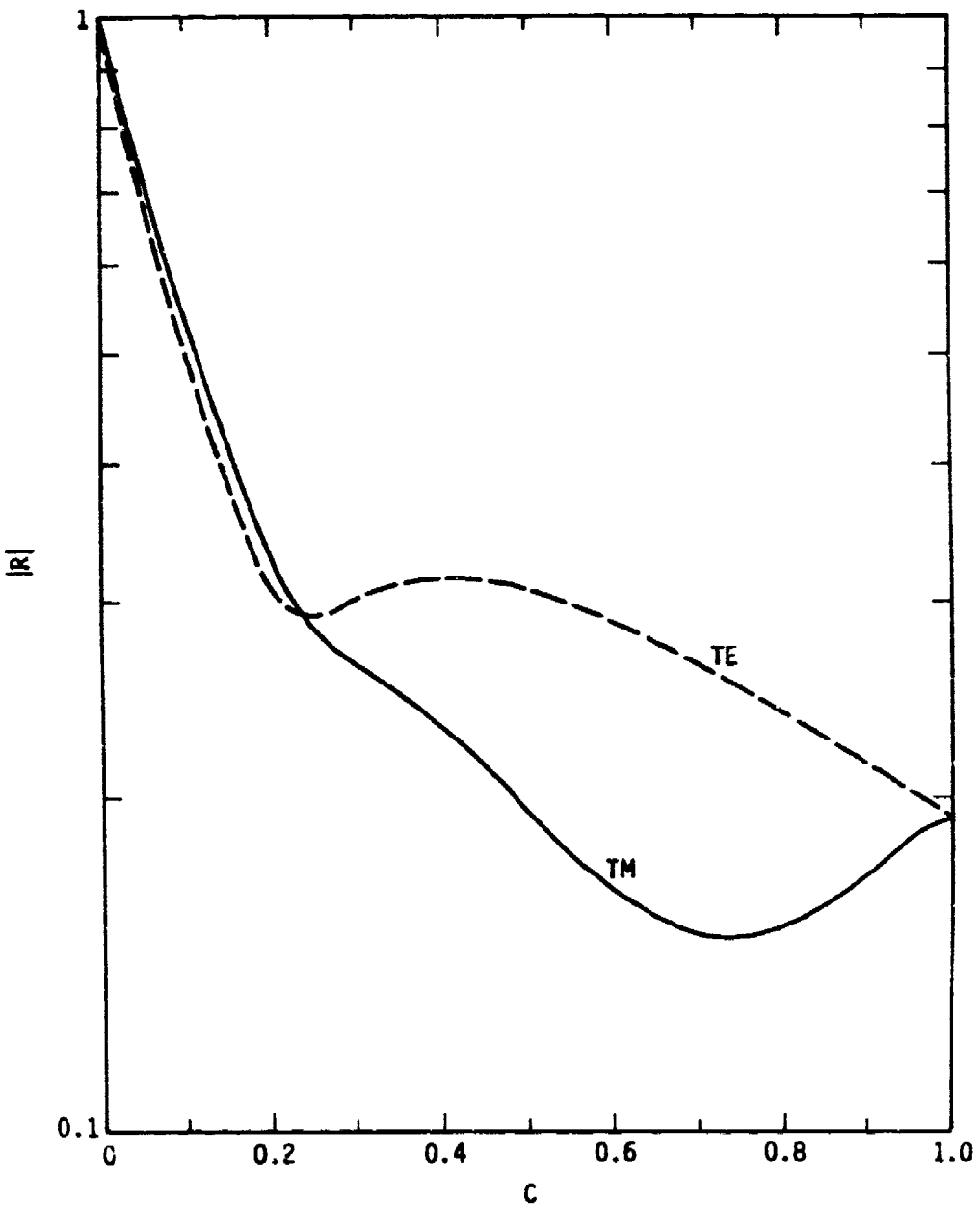

Fig. 19--Retlection coefficients versus incidence angle angle at 20 kHz, W = 2×10^{-11}.

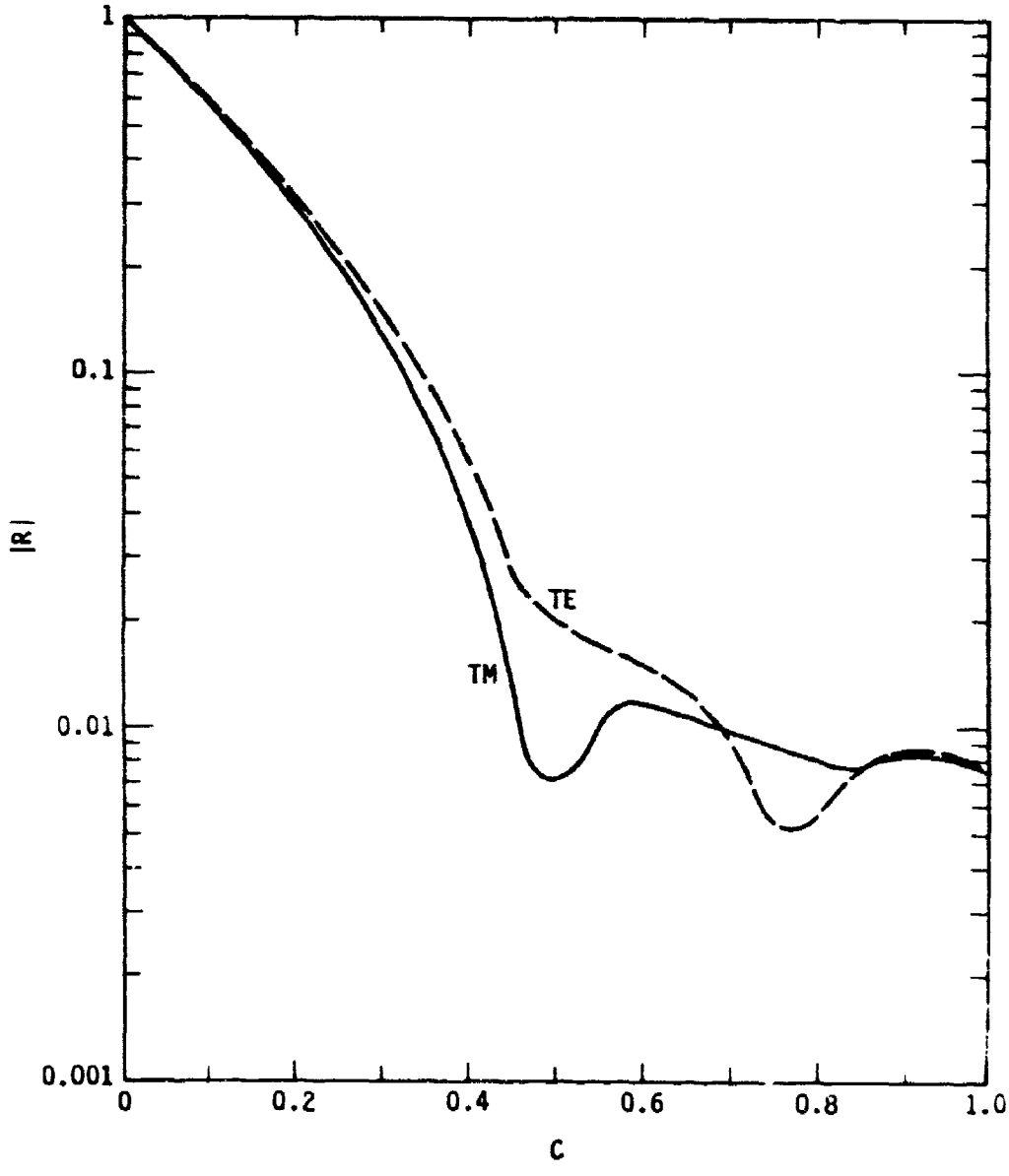

Fig. 20--Reflection coefficients versus incidence angle at 20 kHz, W = 2×10^{-9}.

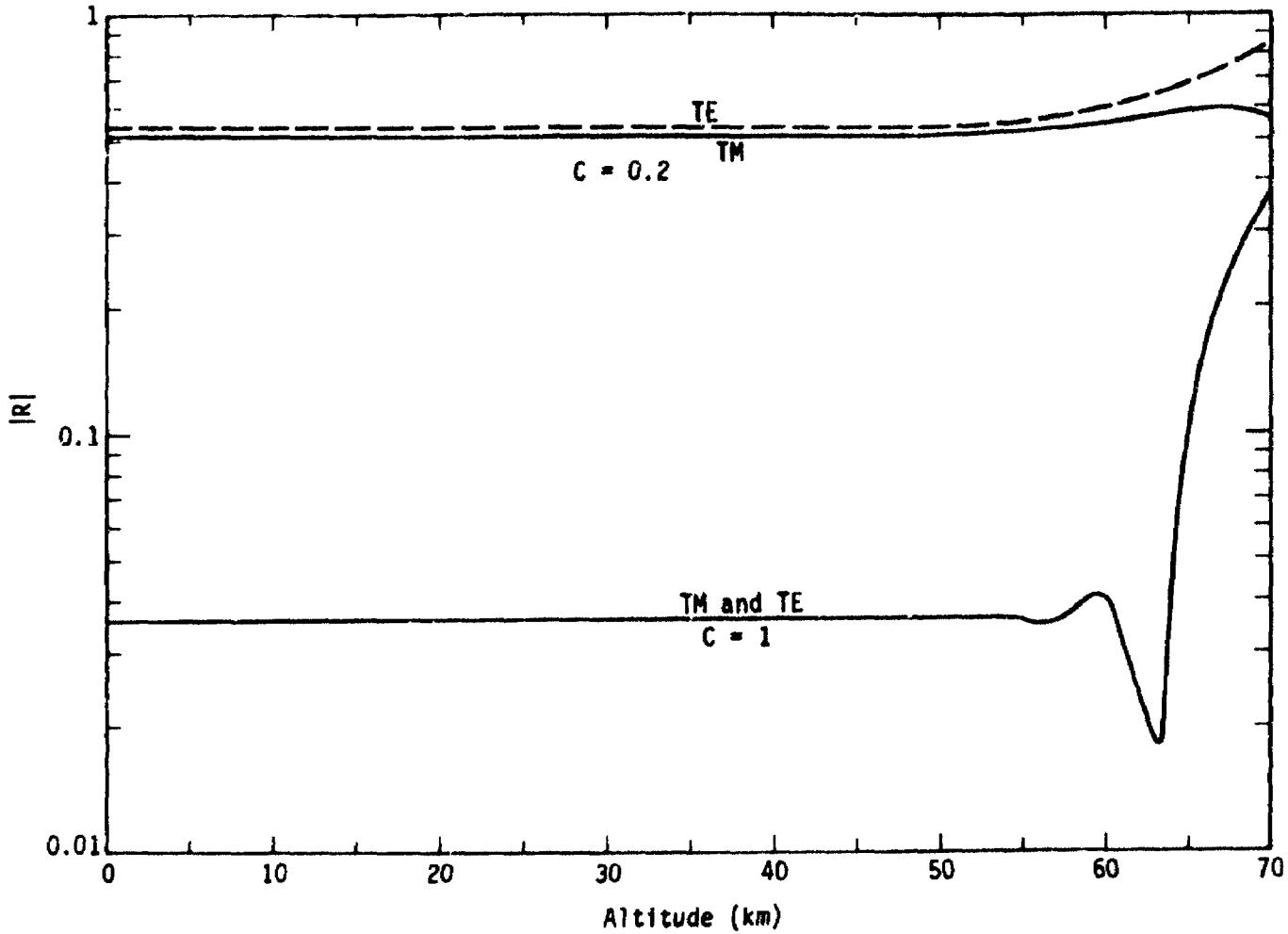

Fig. 21--Reflection coefficients versus altitude for ambient day at 20 kHz.

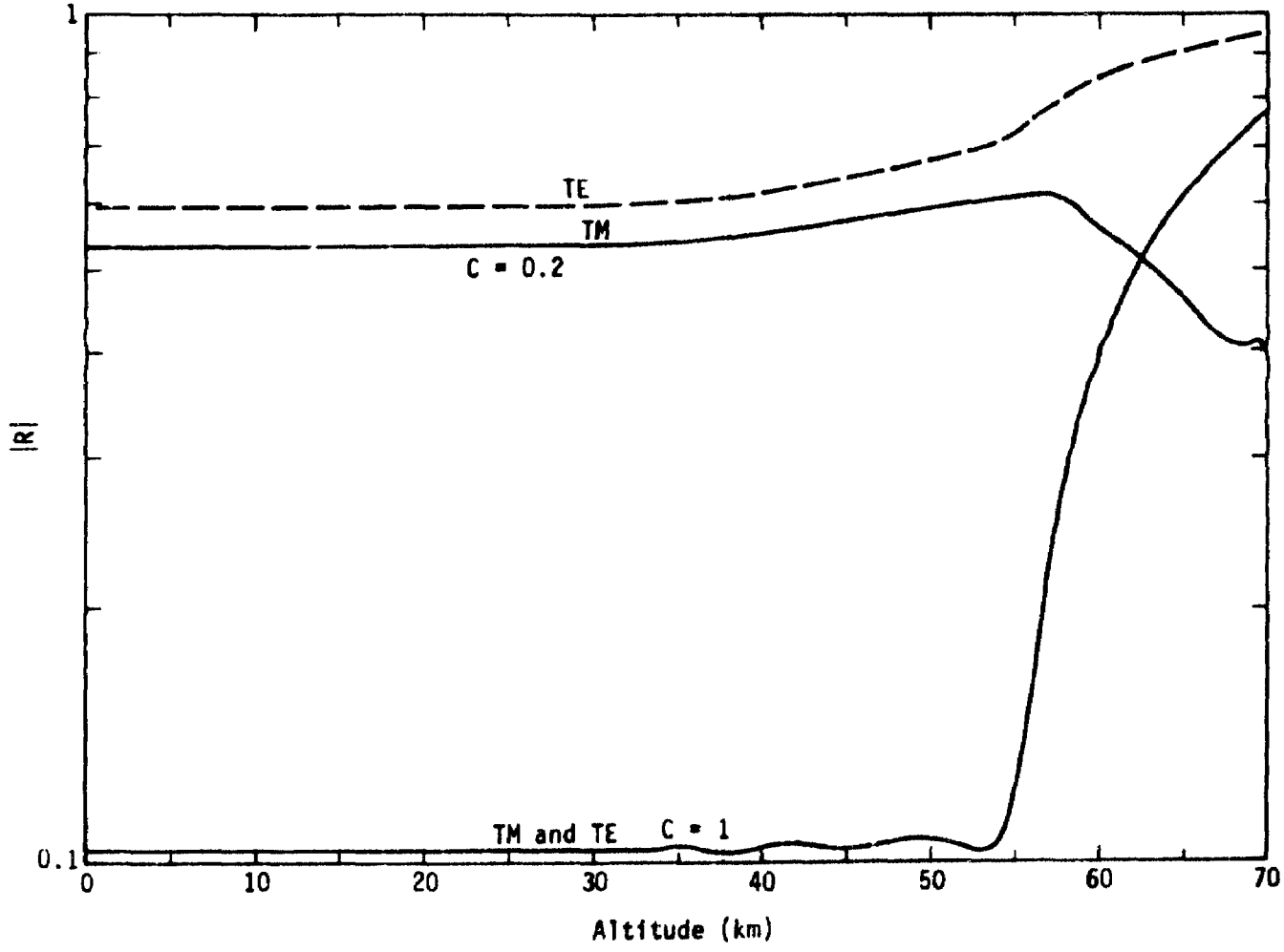

Fig. 22--Reflection coefficients versus altitude for W = 2×10^{-13} and 20 kHz.

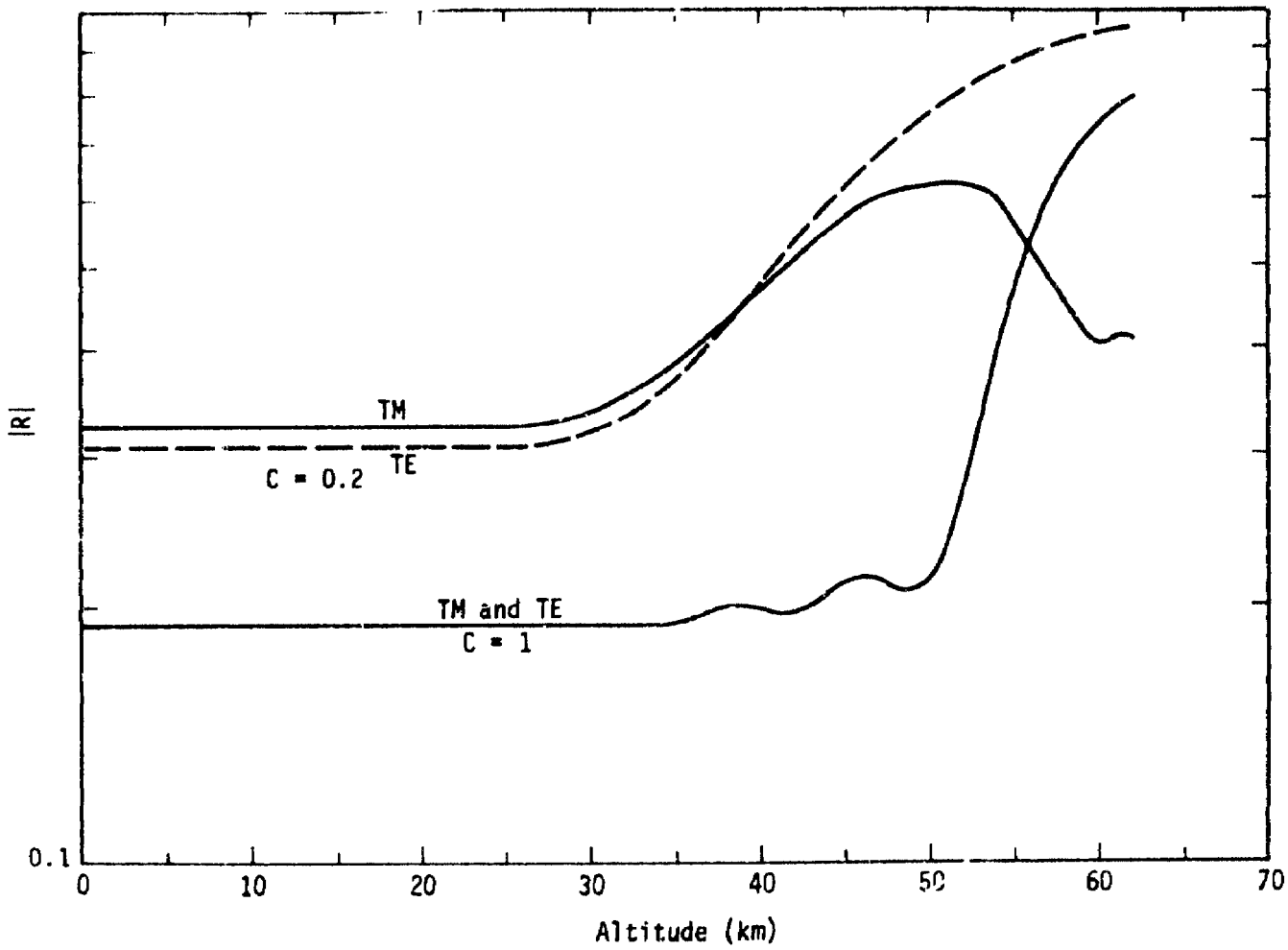

Fig. 23--Reflection coefficients versus altitude for W = 2×10^{-11} and 20 kHz.

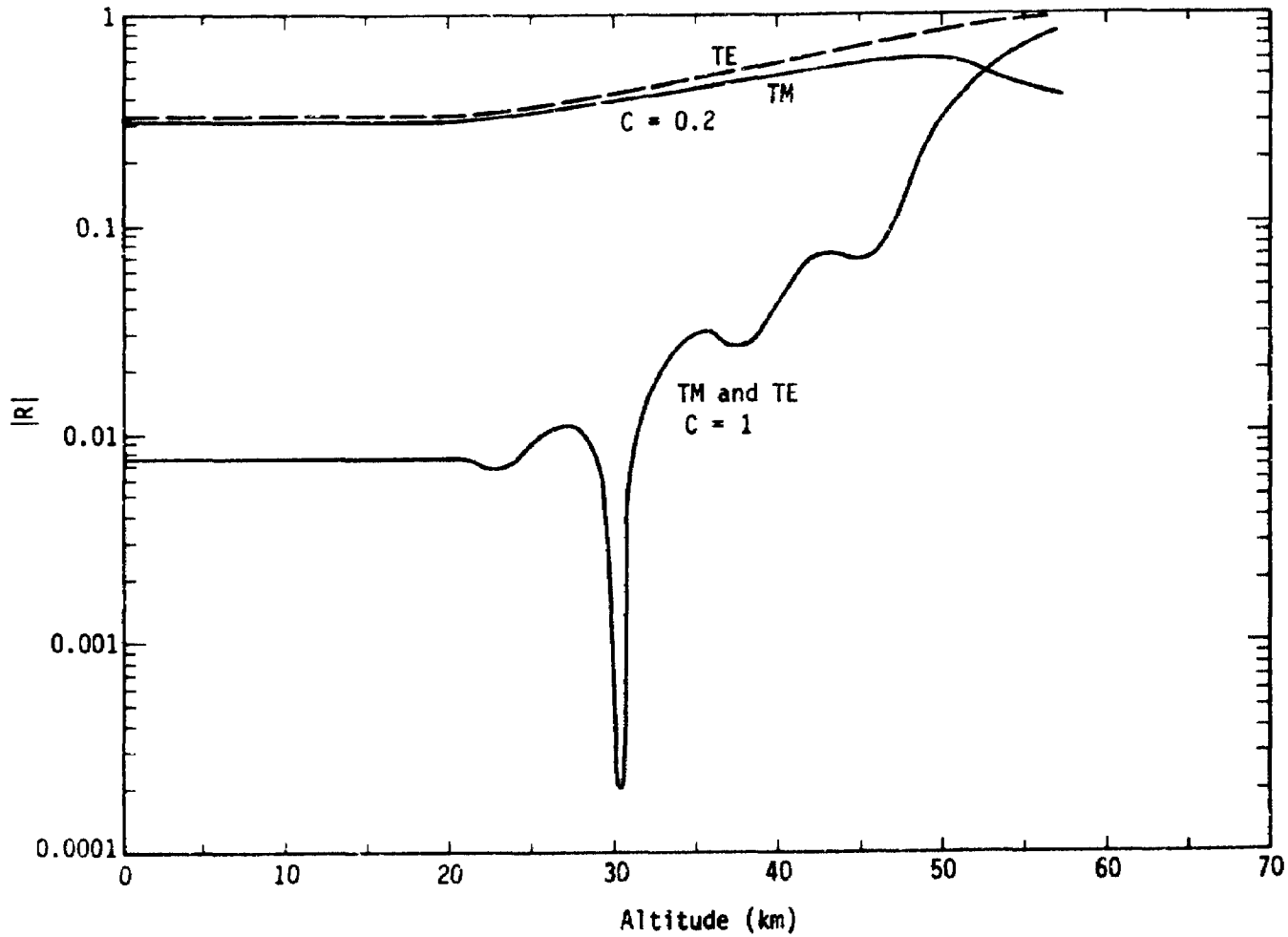

Fig. 24--Reflection coefficients versus altitude for W = 2×10^{-9} and 20 kHz.

of the imaginary part of the squared refractive index, n^2 (see Eq. (A1), p. 48). Accordingly, Fig. 25 shows $Im(n^2)$ versus height for the model ionospheres relevant to Figs. 17 through 20. Field and Engel (*1965*) have shown that most VLF reflection occurs from a 5- or 10-km wide height-region centered at an altitude where

$$Im\ n^2 = \sqrt{2}\ C^2 \quad . \tag{2}$$

Moreover, as shown by Wait (*1970*), if $Im\ n^2$ has the exponential form

$$Im\ n^2 \propto e^{z/H} \quad , \tag{3}$$

where H is the scale-height of the ionospheric conductivity, then the TE-reflection coefficient, R_1, is given by

$$|R_1| = e^{-\pi kHC} \quad , \tag{4}$$

where k is the free-space wave number.

In fact, as shown by Fig. 25, the refractive index is *locally* exponential, having a scale-height that depends on altitude. Consider, for example, the case $W = 2 \times 10^{-9}$. According to Eq. (2), the reflection of a wave with $C = 0.6$ to 0.8 is affected by the 40- to 50-km height-range, where the scale-height is a maximum. According to Eq. (4), one would expect a reflection minimum at these incidence angles. Figure 20 shows that the detailed numerical calculations give such a minimum. Conversely, for ambient conditions, Eq. (2) indicates that the reflection altitudes are above about 50 km for essentially all incidence angles. Since Fig. 25 shows that the ambient scale-height is relatively constant above 50 km, no minimum would be expected in the ambient day

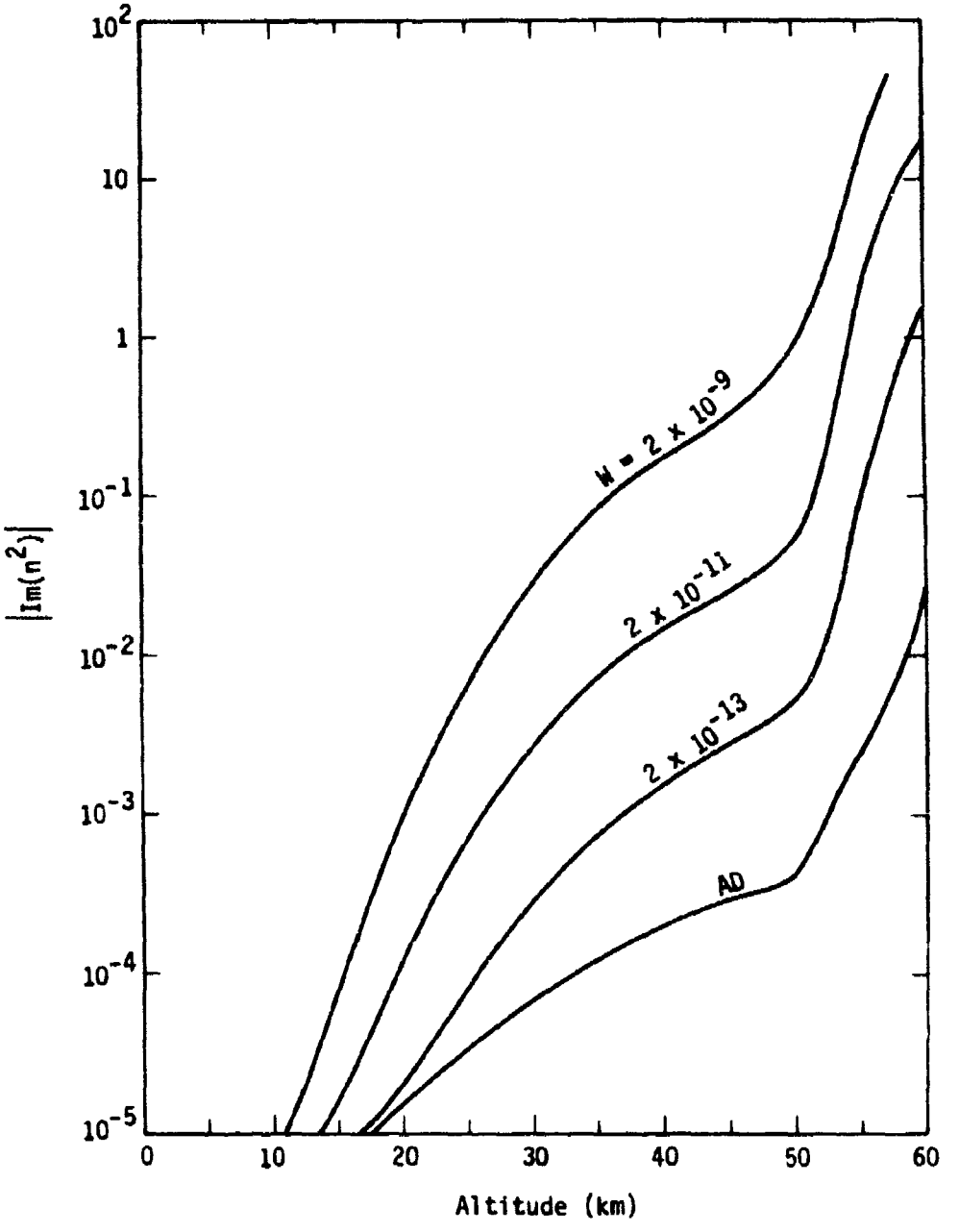

Fig. 25--$Im(n^2)$ versus altitude at 20 kHz for ambient day and three disturbed environments.

TE-reflection coefficient. The numerical results (Fig. 17) again confirm this heuristic conclusion. In summary, the anomalous behavior of the reflection coefficients under moderately or severely disturbed conditions occurs because waves with different incidence angles penetrate to different ionospheric heights, and thus "see" different conductivity gradients.

The results shown in Figs. 17 through 20 must be used with some care since, because of earth curvature, the incidence angle depends on altitude. In fact, since ionospheric reflection does not occur at a well-defined altitude, a well-defined incidence angle cannot be defined. The best one can do is estimate a height, h, that defines the nominal center of the reflection region. Then C as used in Figs. 17 through 20 refers to the incidence angle at the height h. (Of course, according to Eq. (2), h itself depends on C.) If θ_o is the incidence angle at the ground, then the cosine, C, of the ionospheric incidence angle is

$$C = \cos \text{arc} \sin\left[\frac{a}{a+h} \sin \theta_o\right] \quad , \tag{5}$$

where a is the earth's radius; e.g., for a tangentially launched wave ($\theta_o = 90°$) and h = 60 km, C = 0.136.

It is instructive to inquire why the TE mode at 20 kHz is attenuated by about 30 dB/Mm for $W = 2\times10^{-9}$, whereas the TM mode is attenuated by only 10 dB/Mm (Fig. 13). This result may seem puzzling at first, since Fig. 20 shows that the TE- and TM-reflection coefficients are similar at oblique incidence. A simple physical explanation of these numerical results can be given by interpreting the modes as plane

waves having incidence angles equal to the real part of the calculated modal eigenangles.

To satisfy the boundary conditions, the TE mode must be more steeply incident on the ionosphere than the TM mode. For $W = 2 \times 10^{-9}$ and 20 kHz, for example, C was numerically calculated (Eqs. (A7), p. 50, and (A23), p. 54) to be 0.13 and 0.21 for the TM and TE modes, respectively. One consequence of this steeper incidence is that the TE-reflection coefficient is about 3.5 dB smaller than the TM coefficient. More important, however, is the fact that the steeper incidence angle causes the skip distance of the TE-mode plane wave to be only about 350 km, as opposed to about 680 km for that of the TM mode;* i.e., *the TE mode suffers twice as many ionospheric reflections per megameter as the TM mode*. These additional reflections cause most of the excess TE-mode attenuation. Similarly, much of the anomalous attenuation of either mode in disturbed environments is caused by the lowered reflection heights reducing the skip distance. Thus, the attenuation/Mm would increase even if the reflection coefficients were unaltered.

For undisturbed conditions or LF frequencies, both the TE- and TM-mode boundary conditions are satisfied by very oblique launch angles, and the TE-mode skip distance is only slightly smaller than that of the TM mode. Thus, for example, the numerical modal solutions predict only a moderate excess TE-mode attenuation for $W = 2 \times 10^{-13}$ and 40 kHz.

*This skip distance is based on a nominal reflection height-range of 30 to 35 km.

V. RELATIVE IMPORTANCE OF IONS

For the nominal ion mass (29) and ion-collision frequency (ν_i/ν_e = 1/40) used thus far in this report, Eq. (A1) (p. 48) can be used to show that ion terms exceed the electron term in the refractive index if the positive ion density exceeds the electron density by a factor larger than 700. Figure 1 (p. 10) shows that this condition is satisfied at altitudes lower than about 50 km for all model profiles shown. Thus, ions will dominate the propagation in cases where the important reflections occur below about 50 km. Reference to Figs. 21 through 24 shows that, at oblique incidence and $W \leq 2\text{x}10^{-13}$, the reflections occur largely above 50 km and that ions would be expected to play a fairly minor role. Conversely, for $W \geq 2\text{x}10^{-11}$, considerable oblique reflection occurs below 50 km and ions would be expected to play a dominant role.

To quantify the above rather intuitive conclusions regarding the importance of ions, two types of calculations are made with the full-wave modal code described in the appendix. First, the fraction, F_i, of the total joule heating in the ionosphere attributable to ions is calculated. Since, for the models used, the attenuation in the waveguide is due entirely to ionospheric joule heating, F_i represents the fractional contribution of the ions to the attenuation rate. Of course, $1 - F_i$ is the fractional contribution of the electrons. Second, the modal attenuation rates are recalculated using ν_i/ν_e = 1/10 rather than 1/40. Actually, the results of these calculations can be used to determine the sensitivity of the propagation to uncertainties in ion

mass, m_i, and ion density, N_i,* as well as to uncertainties in ν_i. Since the wave angular frequency, ω, is much smaller than ν_i at the altitudes and frequencies of interest, the ionic contribution to the refractive index (Eq. (A1)) is proportional to $N_i/\nu_i m_i$. Thus, a factor-of-four increase in ν_i is equivalent to a factor-of-four increase in m_i, a factor-of-four decrease in N_i, factor-of-two increases in ν_i *and* m_i, etc.

Figure 26 shows F_i versus W for TM and TE modes and frequencies of 20 and 40 kHz. As expected for $\nu_i/\nu_e = 1/40$, ionic heating is the dominant loss mechanism of $W \geq 10^{-12}$, and becomes minor only if ambient conditions are approached ($W < 10^{-13}$). For $\nu_i/\nu_e = 1/10$ (or equivalent changes in m_i and N_i), the effects of ions are considerably reduced, but still become dominant if $W > 10^{-11}$. Ionic losses are generally more pronounced for the TE mode than for the TM mode, albeit by a relatively small amount.

Figure 27 compares TE- and TM-mode attenuation rates at 20 kHz for $\nu_i/\nu_e = 1/40$ and $\nu_i/\nu_e = 1/10$. For $W \leq 10^{-12}$, where electron heating was seen from Fig. 26 to be more important than ion heating, the factor-of-four increase in ion-collision frequency produces only minor changes in attenuation rate. For moderate or strong disturbances ($W \geq 10^{-12}$), the attenuation is considerably reduced for $\nu_i/\nu_e = 1/10$. Note that the TE mode is much more sensitive than the TM mode to changes in ion parameters, with the factor-of-four increase in ν_i causing the TE-mode attenuation to change from 10 dB/Mm to 5 dB/Mm for $W = 10^{-11}$.

---

*Here, N_i is defined as the combined number densities of positive and negative ions.

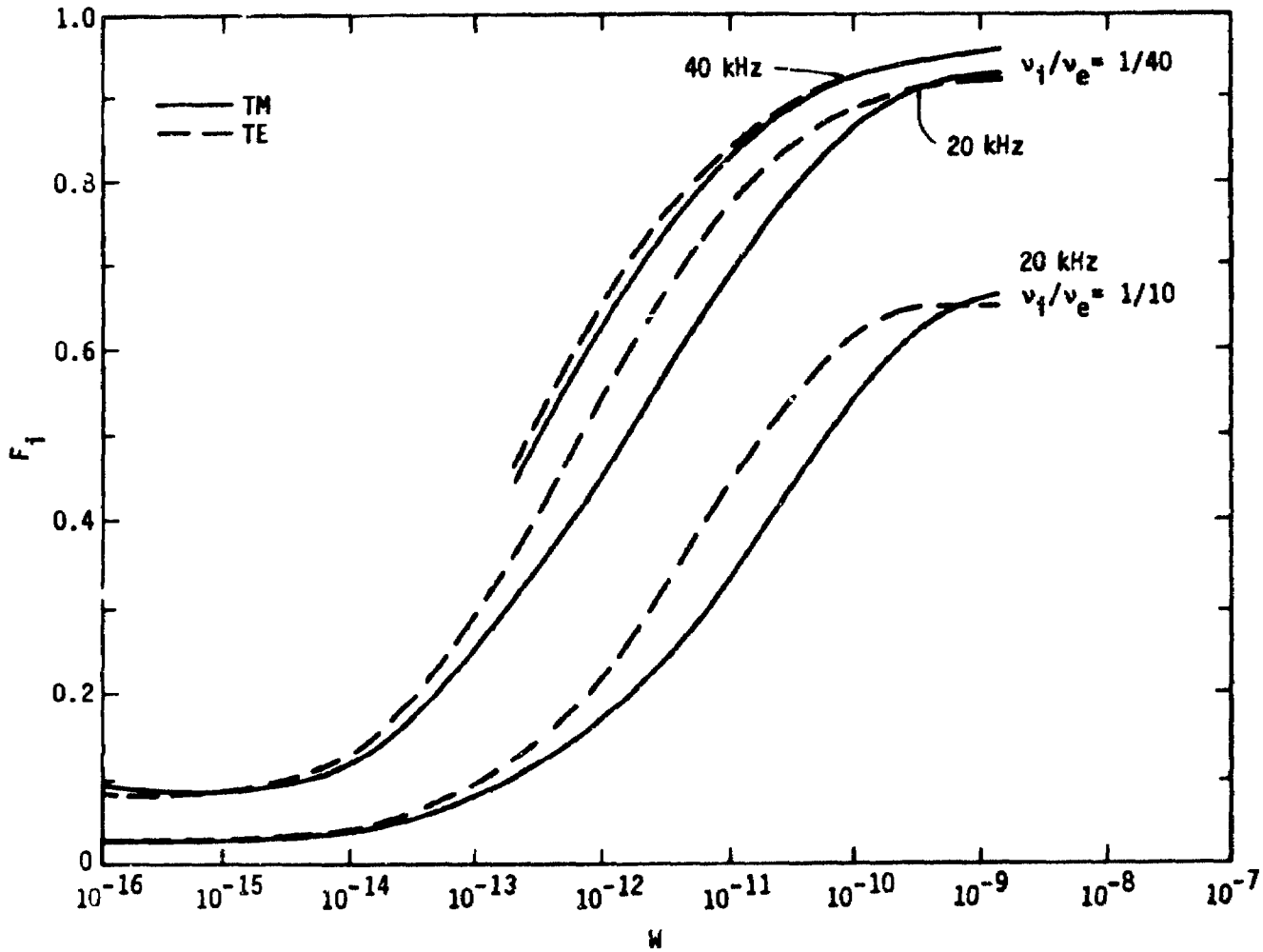

Fig. 26--Fraction of attenuation caused by ion heating.

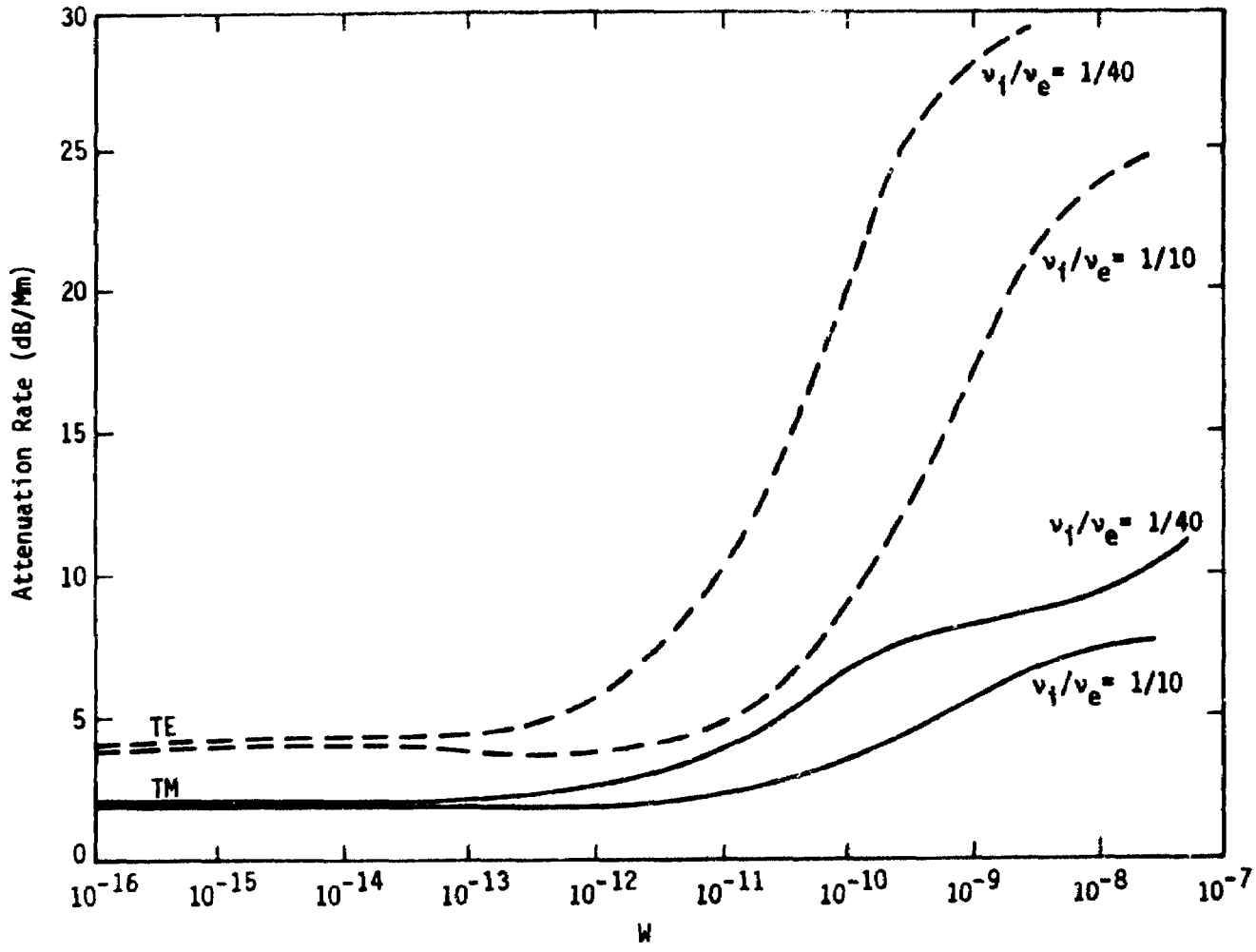

Fig. 27--Comparison of attenuation rates at 20 kHz for two assumed ion-collision-frequency profiles.

Thus, the TE mode would compare much more favorably with the TM mode if the ion-collision frequency or ion mass were larger than assumed in this report and elsewhere (*Knapp and Schwartz, 1975*). Roughly speaking, the factor-of-four uncertainty in ion-collision frequency corresponds to an order of magnitude uncertainty in the ionizing-intensity factor, W.

Appendix

MATHEMATICAL SUMMARY

REFRACTIVE INDEX

For computational purposes, the ionosphere is completely characterized by specifying the complex refractive index throughout the height-regions that govern long-wave propagation in the earth-ionosphere waveguide. This specification requires the number densities, collision frequencies, and masses of each charged species present. Specifically, the refractive index, n, is given by

$$n^2 = 1 - \frac{e^2}{1837\epsilon_o m_e} \sum_{\alpha} \frac{N_\alpha}{\omega(\omega - i\nu_\alpha) q_\alpha} \quad , \qquad \text{(A1)}$$

where ω is the wave angular frequency, ϵ_o is the electric permittivity of free space, e is the electron charge, and m_e is the electron mass. The number density, N_α, collision frequency, ν_α, and atomic mass number, q_α,* of the α^{th} species can be functions of altitude. The effects of the geomagnetic field have not been included in Eq. (A1) since, for the disturbed daytime environments considered in this report, its effects on mode structure are negligible.

WAVEGUIDE MODES

The method used to calculate waveguide mode structure is based on the original formulation of Budden (*1961*), and is described in detail for TM modes by Field (*1970*). Thus, only a brief summary will be given

*$q_\alpha = 1/1837$ for free electrons.

here. A spherical-polar coordinate system is used; the source is located at $\theta = 0$, and the waves travel in the θ-direction. Because azimuthal (ϕ) symmetry is assumed, the ϕ dependence is suppressed throughout. This assumption is valid because the effects of the geomagnetic field on the mode structure are small for the environments considered. Of course, if the excitation factor of the modes were to be calculated, the ϕ dependence would have to be retained except for the case of a purely vertical electric-dipole transmitting antenna. The normalized magnetic intensity $\underline{H} = (\mu_o/\epsilon_o)^{1/2}\underline{H}$ is used, where μ_o is the magnetic permittivity of free space, and $\underline{H}$ is the magnetic intensity. Unless otherwise noted, MKS units are used.

TM Modes

For TM modes, the electric and magnetic fields can be written

$$\underline{E}(\underline{r},\theta) = \left[\hat{e}_r E_r(r,\theta) + \hat{e}_\theta E_\theta(r,\theta)\right] e^{i\omega t} \tag{A2}$$

and

$$\underline{H}(\underline{r},\underline{\theta}) = \hat{e}_\phi H_\phi(r,\theta)\, e^{i\omega t} \quad . \tag{A3}$$

For computational purposes, it is convenient to define the wave admittance,

$$A_{\parallel} \equiv H_\phi/E_\theta \quad , \tag{A4}$$

and the related quantity,

$$W_{\parallel} \equiv \frac{(A_{\parallel}-1)}{(A_{\parallel}+1)} \quad . \tag{A5}$$

By substituting Eqs. (A2) and (A3) into Maxwell's equations and applying the constitutive relations, it follows after some manipulation that W is governed by the following equation:

$$\frac{dW}{dr} = \frac{k}{2i}\left\{n^2(1-W)^2 - \left[1 - \frac{a^2(1-C^2)}{r^2n^2} + \frac{1}{4k^2r^2n^2}\right](1+W)^2\right\} \quad , \qquad (A6)$$

where $k = \omega/c$, c is the vacuum speed of light, a is the earth's radius, and n^2 is given by Eq. (A1). In Eq. (A6), the quantity C can be interpreted as the complex cosine of the incidence angle of the wave at the ground (i.e., at $r = a$). Solution of Eq. (A6) will satisfy the proper boundary conditions for only discrete values, C_N, of C. Hence, C_N is called the eigenvalue of the N^{th} TM mode. For a perfectly conducting earth--the case considered here--the model equation for the eigenvalue is simply

$$W(C_N, r=a) = 1 \quad . \qquad (A7)$$

The data given in Sec. II are sufficient to determine n^2 as a function of height. Once n^2 is determined, Eqs. (A6) and (A7) form a closed set for W and C_N, and are solved by straightforward iteration. Each iteration requires the numerical integration of Eq. (A6), which is started at a great height where a purely upgoing wave is assumed as an initial solution. Thus, since the WKB (eikonal) solution may be used at great heights, the assumed value of W is given in terms of the refractive index, n_o, at the starting height, z_o, by

$$W_{\parallel}(z_o) = \frac{n_o^2 - \sqrt{n_o^2 - (1-C^2)}}{n_o^2 + \sqrt{n_o^2 - (1-C^2)}} \quad , \tag{A8}$$

where the sign of the radical is chosen to correspond to an upgoing wave. In practice, care is taken to choose a starting height so large that C_N is insensitive to its precise value.

Once C_N, and hence $W_{\parallel}(r,C_N)$, have been determined, it is a simple matter to calculate all electromagnetic parameters associated with a given mode. First, it is convenient to define

$$S_N = \left(1-C_N^2\right)^{1/2} \quad . \tag{A9}$$

Then, aside from a geometric spreading term, H_ϕ can be written

$$H_\phi(r=a) \propto \exp[-ikS_N D] \quad , \tag{A10}$$

where D is the path length along the earth's surface. It follows from Eq. (A10) that attenuation rate, η, and phase velocity, V, are given by

$$\eta = 8.7\text{x}10^6 k\ Im\ S \qquad \text{dB/megameter} \tag{A11}$$

and

$$V/c = 1/Re\ S \quad , \tag{A12}$$

where the subscript N has been suppressed. Equations (A10) to (A12) are valid beyond a few e-folding distances from the source and not too near the antipode.

The height-dependences of the fields are found by a straightforward integration of Maxwell's equations, whence, suppressing the time dependence,

$$H_\phi(r) = \frac{a}{r} \exp\left[-ik \int_a^r \frac{n^2(r)}{A(r)}\, dr\right] \quad , \tag{A13}$$

and

$$E_r(r) = -\frac{a}{r} \frac{S}{n^2(r)} H_\phi \quad , \tag{A14}$$

whereas E_θ is found from Eqs. (A4) and (A5). The fields have been normalized such that $H_\phi = 1$ at the ground. The average rate of power dissipation per unit volume is found from Ohm's law to be

$$P_\parallel(r) = \frac{\varepsilon_o \omega}{2} \left(|E_r^2| + |E_\theta^2|\right) Im(1-n^2) \quad . \tag{A15}$$

Again, the subscript N has been suppressed. By using Eq. (A1) in conjunction with Eq. (A15), one can determine the volume rate of power dissipation, $P_\alpha(r)$, associated with each of the α species. The α^{th} species thus absorbs a fraction, F_α, of the total power lost by the N^{th} mode to ionospheric heating, where

$$F_\alpha = \frac{\int_a^\infty P_\alpha(r)\, dr}{\int_a^\infty P_\parallel(r)\, dr} \quad . \tag{A16}$$

From Eqs. (A1), (A15), and (A16), it follows that

$$\sum_{\alpha} F_{\alpha} = 1 \quad .$$

TE Modes

The TE mode fields are

$$\underline{E}(r,\theta) = \hat{e}_{\phi} E_{\phi}(r,\theta)\, e^{i\omega t} \tag{A17}$$

and

$$\underline{H}(r,\theta) = \left[\hat{e}_{r} H_{r}(r,\theta) + \hat{e}_{\theta} H_{\theta}(r,\theta)\right] e^{i\omega t} \quad . \tag{A18}$$

Define

$$A_{\perp} = H_{\theta}/E_{\phi} \tag{A19}$$

and

$$W_{\perp} = \frac{(A_{\perp}-C^2)}{(A_{\perp}+C^2)} \quad , \tag{A20}$$

whence

$$\frac{dW_{\perp}}{dr} = \frac{k}{2i}\left\{C^2(1+W_{\perp})^2 - \frac{n^2}{C^2}\left[1 - \frac{a^2(1-C^2)}{r^2 n^2} + \frac{1}{4k^2 r^2 n^2}\right](1-W_{\perp})^2\right\} \quad . \tag{A21}$$

The starting value for the numerical integration of Eq. (A21) is

$$W_{\perp}(z_o) = \frac{\left(n_o^2 - [1-C^2]\right)^{1/2} + C^2}{\left(n_o^2 - [1-C^2]\right)^{1/2} - C^2} \quad . \tag{A22}$$

The eigenvalue of the m^{th} TE mode is found from

$$W_1(C_m, r=a) = 1 \quad ; \tag{A23}$$

and the formulas for attenuation rate and phase velocity are identical with Eqs. (A9) through (A13) if C_m is substituted for C_N.

The fields are found to be

$$E_\phi(r) = \frac{E_o a}{r} \exp\left[ik \int_a^r A_1(r)\, dr\right] \quad , \tag{A24}$$

$$H_r(r) = -\frac{aS}{r} E_\phi(r) \quad , \tag{A25}$$

and

$$H_\theta(r) = A_1(r) E_\phi(r) \quad , \tag{A26}$$

where E_o is a constant chosen to make $E_\phi = 1$ at the height at which it maximizes--typically, near the effective center of the waveguide for the lowest-order TE mode. The average rate of power dissipation is given by

$$P_1(r) = \frac{\varepsilon_o \omega}{2} \left|E_\phi^2(r)\right| \, Im\left[1-n^2(r)\right] \quad . \tag{A27}$$

Plane-Wave Reflection Coefficients

The calculation of reflection coefficient versus angle of incidence suffers from interpretive difficulties if, as has been done above, the full curvature of the earth is included. In this case, it is difficult

to define an angle of incidence at the ionosphere, since the incidence angle of a given wave changes with height and the lower boundary of the ionosphere is ill-defined. Thus, to permit a unique definition of incidence angle, the wave admittances that enter the expressions for reflection coefficients are calculated from Eqs. (A5), (A6), (A20), and (A21), but in the limit as $a \to \infty$. Noting that $r = a + z$, where z is altitude, it follows that the reflection coefficients referred to $z = 0$ are

$$R_{\parallel}(z) = \frac{CA_{\parallel}(z) - 1}{CA_{\parallel}(z) + 1} e^{-2ikCz} \tag{A28}$$

and

$$R_{\perp}(z) = \frac{C + A_{\perp}(z)}{C - A_{\perp}(z)} e^{-2ikCz} \quad . \tag{A29}$$

In these expressions, C is the cosine of the incidence angle, which is to be specified rather than calculated from the modal boundary conditions. Strictly speaking, $R_{\parallel}$ and $R_{\perp}$ are true reflection coefficients only at altitudes below those at which reflections occur; i.e., below the sensible ionosphere. At altitudes where the inhomogeneous ionosphere strongly affects the propagation, the wave field cannot be decomposed into downgoing and upgoing plane waves. In practical terms, $R_{\parallel}$ and $R_{\perp}$ represent true reflection coefficients at altitudes where they become independent of altitude; i.e., the numerical solutions become independent of z (see Figs. 21 through 24).

REFERENCES

Ali, A. W., W. S. Knapp, and F. E. Niles, "Applications of Computer Solutions to Atmospheric Deionization Processes," Chapter 22, *Reaction-Rate Handbook*, Defense Nuclear Agency, DNA 1948H, Rev. 2, May 1974, p. 22-1.

Budden, K. G., *The Waveguide Mode Theory of Wave Propagation*, Logos Press, London, 1961.

Field, E. C., and R. D. Engel, "The Detection of Daytime Nuclear Bursts Below 150 km by Prompt VLF Phase Anomalies," *Proc. IEEE*, Vol. 53, December 1965, p. 2009.

Field, E. C., "The Effects of Ions on Very-Low-Frequency Propagation During Polar Cap Absorption Events," *Radio Sci.*, Vol. 5, March 1970, p. 591.

Knapp, W. S., and K. Schwartz, *Aids for the Study of Electromagnetic Blackout*, General Electric Company (TEMPO), DNA 3499H, 1 February 1975.

Wait, J. R., *Electromagnetic Waves in Stratified Media*, Pergamon Press, New York, 1970.